Computers and Chemical Engineering 121 (2019) 232–247

Contents lists available at ScienceDirect

Computers and Chemical Engineering

journal homepage: www.elsevier.com/locate/compchemeng

Robust dynamic optimization of enzyme-catalyzed carboligation: A point estimate-based back-off approach

Victor N. Emenike[a,b,c], Xiangzhong Xie[a,b,c], René Schenkendorf[a,b,*], Antje C. Spiess[d], Ulrike Krewer[a,b,*]

[a] Institute of Energy and Process Systems Engineering, Technische Universität Braunschweig, Franz-Liszt-Straße 35, Braunschweig 38106, Germany
[b] PVZ–Center of Pharmaceutical Engineering, Franz-Liszt-Straße 35A, Braunschweig 38106, Germany
[c] International Max Planck Research School for Advanced Methods in Process and Systems Engineering, Sandtorstraße 1, Magdeburg 39106, Germany
[d] Instiute of Biochemical Engineering, Technische Universität Braunschweig, Rebenring 56, Braunschweig 38106 Germany

ARTICLE INFO

Article history:
Received 1 July 2018
Revised 18 September 2018
Accepted 9 October 2018
Available online 25 October 2018

Keywords:
Enzyme catalysis
Benzaldehyde lyase
Optimal reactor design
Back-off strategy
Point estimate method
Dynamic optimization
Robust optimization

ABSTRACT

In this paper, we present a systematic robust dynamic optimization framework applied to the benzaldehyde lyase-catalyzed carboligation of propanal and benzaldehyde to produce (*R*)-2-hydroxy-1-phenylbutan-1-one (BA). First, the elementary process functions approach was used to screen between different dosing concepts, and it was found that simultaneously dosing propanal and benzaldehyde leads to the highest final concentration of BA. Next, we applied global sensitivity analysis and found that 10 out of 13 kinetic parameters are relevant. Time-varying back-offs were then used to handle parametric uncertainties due to these 10 parameters. A major contribution in our work is the use of the point estimate method instead of Monte Carlo simulations to calculate the back-offs in an efficient and reproducible manner. We show that this new approach is at least 10 times faster than the conventional Monte Carlo approach while achieving low approximation errors.

1. Introduction

The need for pharmaceutical processes that are greener, more economical and efficient has led to the consideration of enzyme-catalyzed processes as viable alternatives to chemocatalytic processes (Woodley, 2008). This is mainly due to the high stereoselectivity, and the specificity associated with biocatalytic processes; thus, making it possible to easily and efficiently produce high-quality active pharmaceutical ingredients (APIs) in only a few synthesis steps (Pollard and Woodley, 2007; Woodley, 2008).

C-C bond-forming carboligation is an important reaction in pharmaceutical chemistry because this reaction can be used to prepare pharmaceutically relevant intermediates, such as 2-hydroxy ketones (Hildebrand et al., 2007; Stillger et al., 2006). Traditionally, C-C carboligations are performed via chemocatalysis (Dudding and Houk, 2004; Kokova et al., 2009), but this usually leads to marginal enantiomeric excesses (Hildebrand et al., 2007). Biocatalysis shows higher selectivities and can be used instead of chemocatalysis for performing C-C carboligations (Müller et al., 2013; Stillger et al., 2006; Zavrel et al., 2008). However, for these processes to be economically viable, high product concentration and low enzyme cost should be ensured (Pollard and Woodley, 2007).

To meet these metrics, processes for enzyme-catalyzed carboligations need to be appropriately designed, controlled, and optimized. Better designed, controlled, and optimized biocatalytic processes, in turn, will enable environmental compliance, cost-efficiency, and higher productivity. Mathematical models and computer-aided process systems engineering tools can be used to facilitate the comparison of process variants, the control and optimization of processing conditions, thus reducing the cost and time for process development (Begemann et al., 2016; Pollard and Woodley, 2007).

However, for these models to be of added value for the purposes mentioned above, the models have to be properly calibrated, and the model parameters have to be accurately estimated (Ohs et al., 2017; Schenkendorf et al., 2018; Zavrel et al., 2008). A major issue with the accuracy and validity of mathematical models is the presence of uncertainty in the model parameters (Streif et al., 2016). Therefore, these uncertainties should be taken into account

* Corresponding authors.
E-mail addresses: v.emenike@tu-braunschweig.de (V.N. Emenike), r.schenkendorf@tu-braunschweig.de (R. Schenkendorf), u.krewer@tu-braunschweig.de (U. Krewer).

https://doi.org/10.1016/j.compchemeng.2018.10.006
0098-1354/

in the process development and design phase to avoid issues with poorly designed processes during process operations.

To incorporate uncertainties into the design of enzyme-catalyzed processes, Sin et al. (2009) advocated the use of uncertainty and sensitivity analysis as good modeling practice for biocatalytic processes. In their work, Monte Carlo simulations were used for uncertainty analysis and propagation. For sensitivity analysis, they advised that the local differential sensitivity analysis method should be used for detailed sensitivity analysis, while the global Standardized Regression Coefficients (SRC) method should be used for checking the effect of input parameters on the model outputs. They also suggested that the so-called Morris screening method should be used only when the SRC results are not reliable.

By using the framework proposed by Sin et al. (2009), Price et al. (2014) developed a mechanistic kinetic model for the enzyme-catalyzed transesterification of rapeseed oil in the presence of parametric uncertainties. Although these works (Price et al., 2014; Sin et al., 2009) have made research contributions in uncertainty analysis, they have not addressed how these processes can be designed to be robust to uncertainty.

To address the latter problem, Morales-Rodriguez et al. (2012) proposed a systematic model-based framework for optimization of bioprocesses under uncertainty. Their approach involved applying the SRC method to identify the global sensitivity of the system's output to model parameters. Thus, a smaller subset of the model parameters is selected to reduce the computational overhead. Next, stochastic optimization is performed by using a two-loop Monte Carlo sampling method which involves an outer loop where Latin hypercube sampling is used to determine the sample space of the operating conditions and an inner loop where each of the operating conditions is run over the parametric uncertainty by performing Monte Carlo simulations. A key advantage of their work is that global sensitivity analysis can be used to identify key parameters that can give insights into how to better tune and better design enzymes for bioprocesses. However, a possible challenge with their approach is the high computational cost associated with the Monte Carlo simulations and the stochastic optimization step. This high computational cost makes it difficult to implement such a framework in the context of real-time applications (Aydin et al., 2018).

Furthermore, a key component of most robust optimization formulations are chance constraints which have to be fulfilled for various stochastic instances. In most cases, these chance constraints are transformed into deterministic expressions by using their means and variances (Bergner and Kirches, 2018; Mesbah et al., 2014). A common approximation that is used in this regard is the Cantelli–Chebyshev inequality (Kim and Braatz, 2013; Telen et al., 2015). Even though such approximations have been successfully applied in a number of cases, they do not result in guaranteed bounds for highly nonlinear kinetics and ill-conditioned models that are typically encountered in biocatalysis (Bergner and Kirches, 2018; Paulson and Mesbah, 2017). An example of such bounds is the mean-variance bound, but for a detailed discussion on the bounds mentioned above, please refer to Bergner and Kirches (2018) and references therein.

In order to circumvent such issues, other strategies, such as the back-off strategy, have been shown to be effective (Aydin et al., 2018; Galvanin et al., 2009; Koller et al., 2018; Shi et al., 2016; Visser et al., 2000). The back-off strategy involves tightening violated constraints and shrinking the feasible region such that the worst-case realization of a given process will still be feasible despite variations in the constraints (Shi et al., 2016). Visser et al. (2000) proposed a fast and robust cascade feedback control strategy for batch processes under uncertainty. In their work, the uncertainties were efficiently handled by using a back-off strategy to calculate adequate margins for the path constraints. By using the back-off strategy, the authors showed that a robust cascade feedback controller significantly outperforms an offline control scheme with re-optimizations.

In Srinivasan et al. (2003), an iterative algorithm for robustifying processes by using back-off terms was proposed. This algorithm is initialized by calculating back-off terms from the control inputs of the nominal problem and then iteratively updating the back-offs until a certain convergence criterion is fulfilled.

Another application of the back-off strategy is in the model-based design of experiments (MBDoE). A key paper in this direction is Galvanin et al. (2009) where uncertainty was efficiently handled via time-varying back-offs on relevant constraints during the MBDoE procedure.

Building upon the works of Visser et al. (2000) and Srinivasan et al. (2003), Shi et al. (2016) developed a multistep approach for robust optimization of grade transitions in a polyethylene solution polymerization process in which uncertainties are handled by incorporating back-off constraints. Following the successful application of the multistep back-off algorithm to a detailed large-scale model of an entire flowsheet of the polyethylene polymerization process (Shi et al., 2016), the approach was used for the robust design of a nonlinear model predictive control (NMPC) algorithm for a two-phase hydroformylation semi-batch reactor (Aydin et al., 2018).

The multistep back-off algorithm (Shi et al., 2016) has also been applied to the integrated design, control, and scheduling of multiproduct continuous stirred tank reactor (CSTR) systems in the presence of stochastic process disturbances and parametric noise (Koller et al., 2018). Although previous studies have considered the use of the back-off strategy for integrated design and control, the work by Koller et al. (2018) represents the first attempt to include scheduling as an extra layer of complexity. In their work, two parameters were assumed to be uncertain, namely, the activation energy and the heat of the reaction. In addition to the uncertain parameters, a time-varying stochastic uncertainty in the inlet flow rate (disturbance) to the CSTR was considered. The specific reasons why these parameters were chosen were not mentioned.

Furthermore, Monte Carlo sampling is typically used to estimate the means and variances required for calculating back-off terms. Due to the *weak law of large numbers* (Bertsekas and Tsitsiklis, 2008), numerous Monte Carlo samples are typically required to estimate accurately the true means and variances of random variables. Unfortunately, Monte Carlo sampling does not have a good scaling property and consequently, leads to high computational costs especially when dealing with complex nonlinear models like those encountered in biocatalysis.

In this paper, we propose to reduce this computational overhead by using the point estimate method (Schenkendorf, 2014). We aim to further reduce the computational time by using global sensitivity analysis to identify the parameters that really affect the model output and then propagate the uncertainty of these parameters only. Here, global sensitivity analysis serves as a scientific tool for justifying the relevance of parameters and their uncertainties. Therefore, we present a systematic, robust optimization framework for the carboligation of propanal and benzaldehyde catalyzed by benzaldehyde lyase from *Pseudomonas fluorescens* (*Pf*BAL) to produce (*R*)-2-hydroxy-1-phenylbutan-1-one. This reaction is chosen because it features both self-carboligation and cross-carboligation (Hildebrand et al., 2007; Ohs et al., 2017). Specifically, we aim to maximize the final concentration of (*R*)-2-hydroxy-1-phenylbutan-1-one which is an important intermediate for the synthesis of APIs (Hildebrand et al., 2007; Stillger et al., 2006). In Section 2, we describe the reaction mechanism and kinetics of this reaction. Following this, we describe the methodology in Section 3. First, we screen various intensification cases by using the elementary process functions methodology

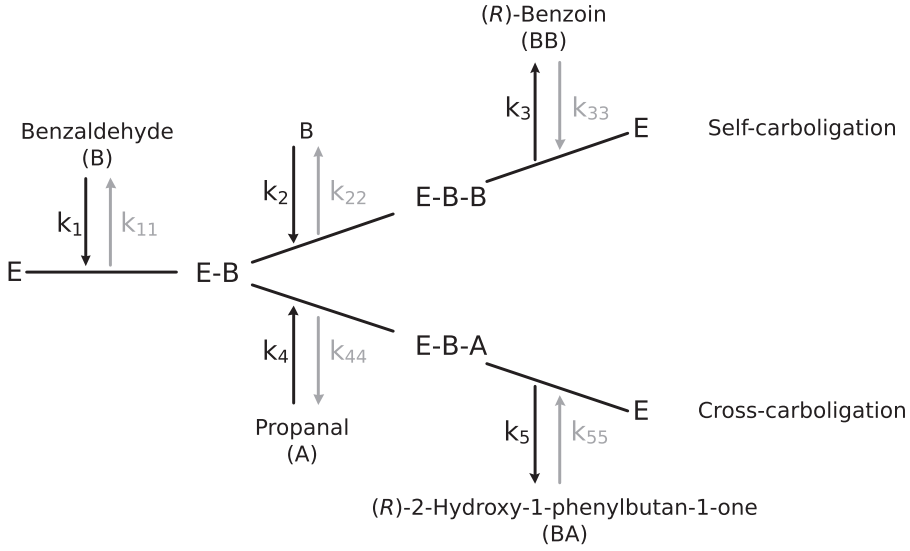

Fig. 1. Branched reaction scheme for *Pf*BAL-catalyzed carboligations with benzaldehyde and propanal as substrates.

(Emenike et al., 2018; Freund and Sundmacher, 2008). Next, we carry out a sensitivity analysis, present the point estimate method, and then delineate the proposed back-off algorithm for robust optimization. In Sections 4 and 5, we apply our systematic approach to the *Pf*BAL catalyzed reaction and discuss the results. Finally, we conclude in Section 6.

2. Problem description

As discussed in the introductory section, we are considering the robust optimization of a *Pf*BAL-catalyzed carboligation reaction in the presence of parametric uncertainty. The reaction mechanism for this reaction is shown in Fig. 1. The reactants are propanal (A) and benzaldehyde (B) which are catalyzed by *Pf*BAL (E) to form (*R*)-2-hydroxy-1-phenylbutan-1-one (BA) and benzoin (BB) as the main product and side product, respectively.

In the first step, B binds to an active site of *Pf*BAL (E) by covalent bonding to form the substrate-enzyme intermediate (E-B). Next, this intermediate branches into two reaction pathways, namely, self-carboligation and cross-carboligation. During self-carboligation, B binds to the E-B intermediate to eventually produce the side product BB. In the cross-carboligation pathway, A reacts with E-B to form the main product BA. Self-carboligation and cross-carboligation are modeled as an ordered bi-uni reaction mechanism.

The mathematical model used to describe these reaction pathways is introduced in Section 2.1. Key elements of this model are parameters which have to be estimated accurately to ensure that the model is feasible for the reactor design and process development. Unfortunately, these parameters are uncertain due to imperfect experimental conditions and inherent measurement errors. Therefore, we need to determine the optimal profiles and conditions that ensure that the derived reactor design is feasible despite parametric uncertainties.

2.1. Reaction kinetics

In this work, we use a relatively detailed kinetic model which consists of equations for the reaction rates for the consumption of propanal and benzaldehyde, the formation of the main product (*R*)-2-hydroxy-1-phenylbutan-1-one and the byproduct benzoin, and very importantly, the rate of inactivation of *Pf*BAL. The details of the model, the parameters and the underlying assumptions are given in Ploch (2014) and Ohs et al. (2018). From hereafter and for the ease of notation, the reaction species propanal, benzaldehyde, (*R*)-2-hydroxy-1-phenylbutan-1-one, the byproduct and *Pf*BAL are denoted as A, B, BA, BB, and E, respectively. The reaction rates for A, B, BA, BB, and E are given as:

$$r_{\mathrm{A}} = -\frac{N_{\mathrm{BA}} C_{\mathrm{E}}}{D \cdot \mathrm{Mwt}_{\mathrm{E}}}, \tag{1}$$

$$r_{\mathrm{B}} = -\frac{(2N_{\mathrm{BB}} + N_{\mathrm{BA}}) C_{\mathrm{E}}}{D \cdot \mathrm{Mwt}_{\mathrm{E}}}, \tag{2}$$

$$r_{\mathrm{BA}} = \frac{N_{\mathrm{BA}} C_{\mathrm{E}}}{D \cdot \mathrm{Mwt}_{\mathrm{E}}}, \tag{3}$$

$$r_{\mathrm{BB}} = \frac{N_{\mathrm{BB}} C_{\mathrm{E}}}{D \cdot \mathrm{Mwt}_{\mathrm{E}}}, \tag{4}$$

$$r_{\mathrm{E}} = \left(-k_{\mathrm{deact,A}} C_{\mathrm{A}} - k_{\mathrm{deact,B}} C_{\mathrm{B}} - k_{\mathrm{deact,time}}\right) C_{\mathrm{E}}, \tag{5}$$

where $\mathrm{Mwt}_{\mathrm{E}}$ is the molecular weight of *Pf*BAL which is equal to 58919 g/mol, while C_i and k_i is the concentration and the kinetic constant of species i, respectively. For ease of representation, the terms N_{BA}, N_{BA}, and D are defined as the following constitutive equations:

$$\begin{aligned} N_{\mathrm{BA}} = {} & k_{22} k_{33} k_4 k_5 C_{\mathrm{A}} C_{\mathrm{BB}} \\ & - k_2 k_3 k_{44} k_{55} C_{\mathrm{B}} C_{\mathrm{BA}} \\ & + k_1 (k_{22} + k_3) k_4 k_5 C_{\mathrm{A}} C_{\mathrm{B}} \\ & - k_{11} (k_{22} + k_3) k_{44} k_{55} C_{\mathrm{BA}}, \end{aligned} \tag{6}$$

$$\begin{aligned} N_{\mathrm{BB}} = {} & k_2 k_3 k_{44} k_{55} C_{\mathrm{B}} C_{\mathrm{BA}} \\ & - k_{22} k_{33} k_4 k_5 C_{\mathrm{A}} C_{\mathrm{BB}} \\ & + k_1 k_2 k_3 (k_{44} + k_5) C_{\mathrm{B}}^2 \\ & - k_{11} k_{22} k_{33} (k_{44} + k_5) C_{\mathrm{BB}}, \end{aligned} \tag{7}$$

Table 1
Reaction kinetic rate parameters (Ploch, 2014).

Rate constant	Value	Unit
k_1	597257.2	$mmol^{-1}L\ min^{-1}$
k_{11}	529,695	min^{-1}
k_2	1,442,733	$mmol^{-1}L\ min^{-1}$
k_{22}	22933.2	min^{-1}
k_3	1264217.4	min^{-1}
k_{33}	1988614.8	$mmol^{-1}L\ min^{-1}$
k_4	3273.6	$mmol^{-1}L\ min^{-1}$
k_{44}	13.8	min^{-1}
k_5	568.8	min^{-1}
k_{55}	56886.6	$mmol^{-1}L\ min^{-1}$
$k_{deact,\ A}$	0.002448	$mmol^{-1}L\ min^{-1}$
$k_{deact,\ B}$	0.001632	$mmol^{-1}L\ min^{-1}$
$k_{deact,\ time}$	0.000112	min^{-1}

$$
\begin{aligned}
D = {} & k_{11}(k_{22}+k_3)(k_{44}+k_5) \\
& + k_1(k_{22}+k_3)k_4 C_A C_B \\
& + (k_{22}+k_3)k_4 k_{55} C_A C_{BA} \\
& + k_{33}k_4(k_{22}+k_5)C_A C_{BB} \\
& + k_1 k_2 (k_{44}+k_5) C_B^2 \\
& + k_2(k_3+k_{44})k_{55} C_B C_{BA} \\
& + k_2 k_{33}(k_{44}+k_5) C_B C_{BB} \\
& + (k_{22}+k_3)k_4 k_5 C_A \\
& + k_1(k_{22}+k_3)(k_{44}+k_5)C_B \\
& + k_2 k_3 (k_{44}+k_5) C_B \\
& + (k_{11}+k_{44})(k_{22}+k_3)k_{55} C_{BA} \\
& + (k_{11}+k_{22})k_{33}(k_{44}+k_5)C_{BB}. \qquad (8)
\end{aligned}
$$

All kinetic parameters in Eqs. (6)–(8) are summarized in Table 1.

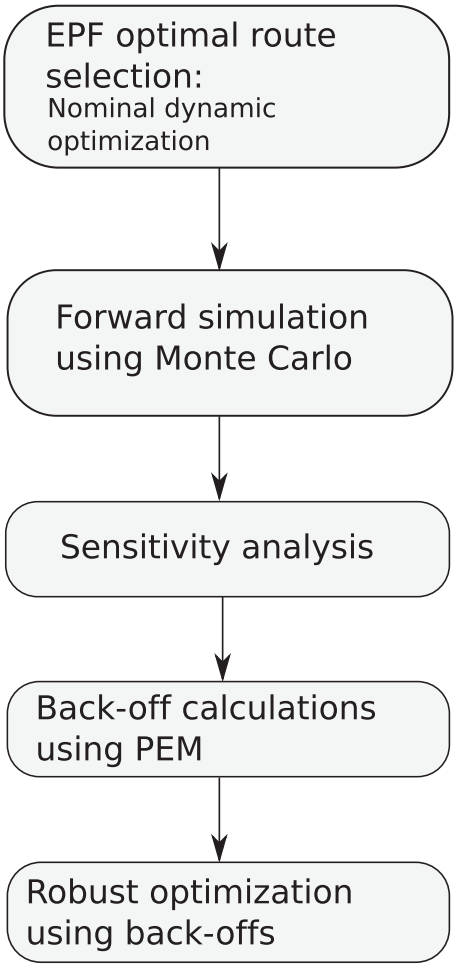

Fig. 2. Workflow of the robust optimization strategy.

3. Methodology

In this section, we introduce and describe the key components of our robust optimization framework which is graphically summarized in Fig. 2. First, the elementary process function (EPF) approach is introduced as a method to determine the optimal reaction route by considering different intensification cases. The EPF approach inherently leads to a dynamic optimization problem, and thus, the dynamic optimization solution technique that we employ is also described. The best intensification case from the EPF step is then selected and analyzed in more detail. Next, forward realizations of the best intensification case are performed at Monte Carlo (parameter) sample points. This is done to determine which constraints are violated for the different parameter realizations. Once these constraints are determined, we then focus on robustifying these constraints (Puschke et al., 2017).

Subsequently, global sensitivity analysis is applied to select the relevant parameters that affect the states associated with the constraints which were violated in the previous step. Next, the best intensification case is robustified by using a time-varying back-off strategy. A major novelty in our work is the use of the point estimate method (PEM) instead of Monte Carlo simulations to calculate the statistical moments required for the back-off calculations. As a result, the PEM is briefly described and then followed by a detailed explanation of the PEM-based back-off algorithm. Finally, we describe how we compare the accuracy of our approach with the Monte Carlo–based approach by using the root-mean-square prediction error.

3.1. Optimal reaction route selection: elementary process functions

The EPF methodology proposed by Freund and Sundmacher (2008) differentiates itself from the conventional unit operation approach in process design that is based on and therefore limited to “off-the-shelf” processing units. Within the EPF framework, these units are replaced by functional modules in which the states of a passing fluid element are changed by fluxes, such as heat, mass, component dosing, and diffusion fluxes. Mathematically, the fluid element is represented as (Freund and Sundmacher, 2008):

$$\frac{d\mathbf{x}}{dt} = \sum_{k=1}^{J} j_k^{\Phi}(\mathbf{x}) \cdot \mathbf{e}_k, \qquad (9)$$

where $\mathbf{x}$ is a state vector (e.g., mass, energy, concentration), j_k^{Φ} is the flux k of the functional module Φ, $\mathbf{e}_k$ is the EPF of flux k (i.e., a basis vector in thermodynamic state space), and J is the total number of fluxes of the functional module Φ. The EPF $\mathbf{e}_k$ represents a specific direction of flux k in thermodynamic state space, and the combined effect of the EPFs determines the region in thermodynamic state space that is attainable by the fluid element (see Freund and Sundmacher (2008) for details).

The fluid element traveling through the functional modules is then tracked to find the optimal route in state space. Next, the optimal route is technically realized by using existing process units or by designing new apparatuses (Peschel et al., 2010). In

this work, we consider only the first level of EPF as described in Peschel et al. (2010).

3.2. Dynamic optimization

The design problem within the EPF framework translates into a dynamic optimization problem where fluxes flowing in and out of the fluid element are optimized as the fluid element is tracked in thermodynamic state space. In this work, we focus on a Mayer-type problem (Biegler, 2010) with the following general form:

$$\begin{aligned} \underset{\mathbf{x}(\cdot),\mathbf{u}(\cdot),\mathbf{z}(\cdot)}{\text{minimize}} \quad & \Phi(\mathbf{x}(t_\mathrm{f})) \\ \text{subject to} \quad & \dot{\mathbf{x}}(t) = \mathbf{f}(\mathbf{x}(t),\mathbf{z}(t),\mathbf{u}(t),\boldsymbol{\theta}), \quad \forall t \in \mathcal{T}, \\ & \mathbf{g}(\mathbf{x}(t),\mathbf{z}(t),\mathbf{u}(t),\boldsymbol{\theta}) = \mathbf{0}, \quad \forall t \in \mathcal{T}, \\ & \mathbf{h}(\mathbf{x}(t),\mathbf{z}(t),\mathbf{u}(t),\boldsymbol{\theta}) \leq \mathbf{0}, \quad \forall t \in \mathcal{T}, \\ & \mathbf{x}(t_0) = \mathbf{x}_0\,, \\ & \mathbf{u}(t) \in \mathcal{U}\,, \end{aligned} \tag{10}$$

on the time horizon $\mathcal{T} := [t_0, t_\mathrm{f}] \subset \mathbb{R}$ of the enzyme catalytic reaction, where t_0 and t_f are the initial and final time points, respectively. The control vector $\mathbf{u} \in \mathbb{R}^{n_u}$ is an element of the admissible set of controls $\mathcal{U}$; $\Phi(\mathbf{x}(t_\mathrm{f}))$ is an objective function which is to be minimized (or maximized), e.g., final product concentration, space time yield, or total enzyme turnover number; $\mathbf{x}(t) \in \mathbb{R}^{n_\mathrm{x}}$ is a vector of state variables which, in this case, are species amounts or concentrations; $\mathbf{z}(t) \in \mathbb{R}^{n_z}$ is a vector of algebraic variables, such as the reaction rates; $\boldsymbol{\theta} \in \mathbb{R}^{n_\theta}$ is a vector of time-independent parameters; $\mathbf{f} : \mathcal{T} \times \mathbb{R}^{n_\mathrm{x}} \times \mathbb{R}^{n_u} \times \mathbb{R}^{n_z} \times \mathbb{R}^{n_\theta} \to \mathbb{R}^{n_\mathrm{x}}$ is a function vector that defines the derivatives of the states; $\mathbf{g} : \mathcal{T} \times \mathbb{R}^{n_\mathrm{x}} \times \mathbb{R}^{n_u} \times \mathbb{R}^{n_z} \times \mathbb{R}^{n_\theta} \to \mathbb{R}^{n_\mathrm{g}}$ is a function vector that defines the equality constraints; $\mathbf{h} : \mathcal{T} \times \mathbb{R}^{n_\mathrm{x}} \times \mathbb{R}^{n_u} \times \mathbb{R}^{n_z} \times \mathbb{R}^{n_\theta} \to \mathbb{R}^{n_\mathrm{h}}$ is the inequality (path) constraint function vector; and $\mathbf{x}_0$ is a vector of the initial conditions of the states at initial time t_0 which could also be decision variables.

3.3. Dynamic optimization solution strategy: direct collocation

To solve the infinite dimensional dynamic optimization problem (10), we employ the simultaneous approach where we discretize the states and controls of the problem (10) to get a finite-dimensional nonlinear programming (NLP) problem (Biegler, 1984; Cuthrell and Biegler, 1987). The simultaneous approach was selected because of its ability to handle numerical instabilities and path constraints efficiently (Biegler, 2007; 2010). In particular, we use a direct collocation method where the time horizon is discretized into finite elements N with each element containing K collocation points. Here, the states and algebraic variables are discretized on the finite elements and the collocation points by parameterizing them with orthogonal polynomials on Radau collocation points, while the controls are discretized on only the finite elements by using a piecewise constant parameterization. We first define an ordered set of indices for the finite elements as $\mathcal{F} = \{1, \ldots, N\}$ and that of the collocation points as $\mathcal{C} = \{1, \ldots, K\}$ and then present the discretized form of problem (10) as the following NLP problem:

$$\underset{\hat{\mathbf{x}},\hat{\mathbf{u}},\hat{\mathbf{z}}}{\text{minimize}} \ \Phi(\mathbf{x}_\mathrm{N}) \tag{11a}$$

$$\text{subject to} \quad \dot{\mathbf{x}}_{i,j} = \mathbf{f}(\mathbf{x}_{i,j}, \mathbf{z}_{i,j}, \mathbf{u}_i, \boldsymbol{\theta}), \qquad \forall i \in \mathcal{F},\ j \in \mathcal{C} \tag{11b}$$

$$\mathbf{x}_{i,j} = \mathbf{x}_i + \sum_{k=1}^{K} \boldsymbol{\Omega}_{k,j} \dot{\mathbf{x}}_{i,j}, \qquad \forall i \in \mathcal{F},\ j \in \mathcal{C} \tag{11c}$$

$$\mathbf{g}(\mathbf{x}_{i,j}, \mathbf{z}_{i,j}, \mathbf{u}_i, \boldsymbol{\theta}) = \mathbf{0}, \qquad \forall i \in \mathcal{F},\ j \in \mathcal{C} \tag{11d}$$

$$\mathbf{h}(\mathbf{x}_{i,j}, \mathbf{z}_{i,j}, \mathbf{u}_i, \boldsymbol{\theta}) \leq \mathbf{0}, \qquad \forall i \in \mathcal{F},\ j \in \mathcal{C} \tag{11e}$$

$$\mathbf{x}_1 = \mathbf{x}_0 \tag{11f}$$

$$\mathbf{x}_{i+1} = \mathbf{x}_{i,K}, \qquad \forall i \in \mathcal{F} \backslash \{N\}. \tag{11g}$$

For the sake of a compact representation of the decision variables, the discretized states, algebraic variables, and controls are collected into separate vectors:

$$\hat{\mathbf{x}} := \begin{bmatrix} \mathbf{x}_1 \\ \mathbf{x}_{1,1} \\ \vdots \\ \mathbf{x}_{N,K-1} \\ \mathbf{x}_N \end{bmatrix}, \qquad \hat{\mathbf{z}} := \begin{bmatrix} \mathbf{z}_{1,1} \\ \vdots \\ \mathbf{z}_{N,K-1} \\ \mathbf{z}_{N,K} \end{bmatrix}, \qquad \hat{\mathbf{u}} := \begin{bmatrix} \mathbf{u}_1 \\ \vdots \\ \mathbf{u}_N \end{bmatrix},$$

with $\mathbf{x}_i, \mathbf{x}_{i,j} \in \mathbb{R}^{n_\mathrm{x}}$, $\mathbf{z}_{i,j} \in \mathbb{R}^{n_z}$, and $\mathbf{u}_i \in \mathbb{R}^{n_u}$. The discretized form of the Mayer-type objective function (11a) is now defined at the last finite element N and collocation point K as $\Phi(\mathbf{x}_\mathrm{N})$, and Eq. (11b) represents the discretized differential states. Furthermore, the collocation equations over the finite elements $i \in \mathcal{F}$ and collocation points $j \in \mathcal{C}$ are defined by Eq. (11c). These equations utilize parameters from the collocation matrix $\boldsymbol{\Omega}$ which is derived from an orthogonal polynomial of order K with roots at Radau collocation points (Biegler, 2010). Eqs. (11d) and (11e) define the equality constraints and path constraints over $i \in \mathcal{F}$ and $j \in \mathcal{C}$, respectively. Finally, Eq. (11f) defines the initial point, while Eq. (11g) enforces the continuity of the differential profiles.

3.4. Sensitivity analysis

Global sensitivity analysis (GSA) is a useful technique for analyzing processes and has been applied in various studies. Although not mandatory for the robust optimization framework, GSA enables us to gain knowledge about the relations between parameters and the model output, especially the impact of parameter uncertainties on the variation of the model output. GSA assists us in figuring out the most relevant parameters and which parameter uncertainties must be considered for the robust optimization. While focusing on the relevant parameters and neglecting the irrelevant one, we can reduce the complexity of the robust optimization problem considerably.

The frequently used Sobol' indices approach, which is a variance-based method, is implemented in this study. Sobol' indices are used because they provide a more comprehensive definition of the sensitivities of model outputs to parameters and the interactions between these parameters. Please note that the sum of all the Sobol' indices is equal to unity. The Sobol' indices were first proposed in Sobol (1993) and have been applied in various studies in different disciplines (Boukouvala et al., 2012; Ciriello et al., 2013; Kiparissides et al., 2009; Lin et al., 2018; Rehrl et al., 2017; Saltelli et al., 2000; Schenkendorf et al., 2018; Wang and Ierapetritou, 2018). Three sensitivity indices are introduced to characterize the effect of parameters on the model output, which are the first-order sensitivity indices S_i, the interaction sensitivity indices $S_{i,j,\ldots}$, and total sensitivity indices S_{T_i}. The first-order and interaction sensitivity indices give quantitative information about the effect of a single parameter i and the effect of interactions among parameters $i, j, \ldots$ on the model output, respectively, while the total sensitivity indices give quantitative information about the overall effect of a parameter i on the model output, including parameter interactions. The total sensitivity indices are equal to the sum of its first-order sensitivity indices and all other interaction sensitivities where it is included. Therefore, only the first-order and total sensitivity indices are calculated in this work to screen for relevant parameters. For details regarding procedures and formulas used to calculate the

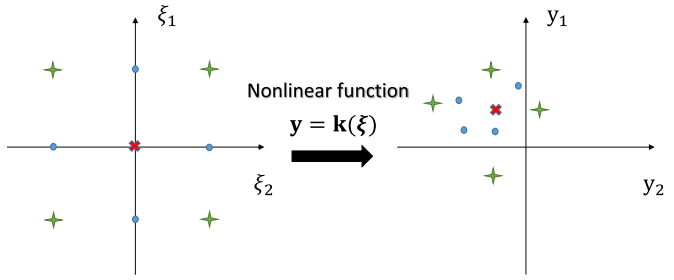

Fig. 3. Illustration of the PEM for a nonlinear function $\mathbf{y} = \mathbf{k}(\boldsymbol{\xi})$ which has two random inputs ξ_1, ξ_2 and two random outputs y_1, y_2 (Julier and Uhlmann, 1996).

sensitivities, please refer to Lin et al. (2018) and Xie et al. (2018b). The sensitivity indices have been calculated with UQLAB developed at ETH Zürich (Marelli and Sudret, 2014).

3.5. Point estimate method

Before demonstrating the robust optimization approach, we introduce the point estimate method (PEM) which we use instead of Monte Carlo simulations to estimate the means (expected values) and variances required to calculate the time-varying back-offs $\mathbf{b}_c(t)$. The PEM approximates the statistical moments of a random variable based on a reasonable number of deterministic sample points (Lerner, 2002; Schenkendorf, 2014; Xie et al., 2018a). The basic principle of the PEM is illustrated in Fig. 3. Specially picked points for random parameters are transferred through a nonlinear function, and the integral of the output can be then approximated by a weighted superposition of the realizations as:

$$\int_{\mathbb{I}_\xi} \mathbf{k}(\boldsymbol{\xi}) f(\boldsymbol{\xi}) d\boldsymbol{\xi} \approx \sum_{i=1}^{n_p} w_i \mathbf{k}(\boldsymbol{\xi}_i^s), \qquad n_p = 2n_\xi^2 + 1, \tag{12}$$

where $k(\cdot)$ presents the nonlinear function, $f(\boldsymbol{\xi})$ is the probability density function of the random parameter vector $\boldsymbol{\xi}$, $\boldsymbol{\xi}_i^s$ are the deterministic sample points which has a number of n_p, and w_i are the weights that depend on the distribution we have for the random parameters. In order to establish Eq. 12, the distribution of the parameters has to be symmetric over 0, and thus, the standard normal distribution is typically assumed and used to compute the weights. However, it can also be extended to any arbitrary or even correlated distribution by using an isoprobabilistic transformation approach (Xie et al., 2018a).

The PEM-generator function GF[·] defined in Lerner (2002) is used to generate deterministic sample points for a standard normal distribution, which also determines the overall number of sample points, i.e., $2n_\xi^2 + 1$. For all combinatorial realizations, the generator function substitutes zero, one, and two elements of a given random parameter vector with GF[0], GF[$\pm\vartheta$], and GF[$\pm\vartheta$, $\pm\vartheta$], respectively, where ϑ controls the spread of the permutation. For more details concerning the generator function, the interested reader is referred to Lerner (2002) and references therein. In robust process design, we are interested in the first and second statistical moments which correspond to the expected value and the variance, respectively. Therefore, by using the PEM we obtain the expected value of the function $\mathbf{k}(\boldsymbol{\xi})$ by rewriting Eq. 12 as:

$$\begin{aligned}\mathbb{E}[\mathbf{k}(\boldsymbol{\xi})] = \int_{\mathbb{I}_\xi} \mathbf{k}(\boldsymbol{\xi}) f(\boldsymbol{\xi}) d\boldsymbol{\xi} \approx w_0 \mathbf{k}(GF[0]) + w_1 \sum \mathbf{k}(GF[\pm\vartheta]) \\ + w_2 \sum \mathbf{k}(GF[\pm\vartheta, \pm\vartheta]),\end{aligned} \tag{13}$$

where the position parameter and weight factors are $\vartheta = \sqrt{3}, w_0 = 1 + \frac{d^2-7d}{18}, w_1 = \frac{4-d}{18}, w_2 = \frac{1}{36}$. In the same vein, the variance can be estimated with the following equation:

$$\begin{aligned}\mathrm{Var}[\mathbf{k}(\boldsymbol{\xi})] = \int_{\mathbb{I}_\xi} (\mathbf{k}(\boldsymbol{\xi}) - \mathbb{E}[\mathbf{k}(\boldsymbol{\xi})])^2 f(\boldsymbol{\xi}) d\boldsymbol{\xi} \approx w_0 (\mathbf{k}(GF[0]) \\ - \mathbb{E}[\mathbf{k}(\boldsymbol{\xi})])^2 + w_1 \sum (\mathbf{k}(GF[\pm\vartheta]) - \mathbb{E}[\mathbf{k}(\boldsymbol{\xi})])^2 \\ + w_2 \sum (\mathbf{k}(GF[\pm\vartheta, \pm\vartheta]) - \mathbb{E}[\mathbf{k}(\boldsymbol{\xi})])^2,\end{aligned} \tag{14}$$

3.6. Robust dynamic optimization

As already discussed, the typical robust optimization is more challenging to apply for reactor design problems involving enzyme-catalyzed reactions. This is due to the complex kinetic equations and possible ill-conditioned model equations. As such, we adopt the concept of back-off constraints to handle parametric uncertainties (Shi et al., 2016; Srinivasan et al., 2003).

For the back-off strategy, we first consider the inequality (path) constraints defined in problem (10):

$$\mathbf{h}(\mathbf{x}(t), \mathbf{z}(t), \mathbf{u}(t), \boldsymbol{\theta}) \leq \mathbf{0}. \tag{15}$$

Second, we ensure that the path constraints are fulfilled in the presence of uncertainties by introducing time-varying back-off terms to the constraints at the nominal parameter vector $\bar{\boldsymbol{\theta}}$.

Please note that constant back-off terms could also be used. In such a case, the value of the constant back-off terms will be set to the maximum variability (margin) across the time domain. We are in favor of time-varying back-offs as they lead to less conservative robust solutions than when constant back-off terms are used (Koller et al., 2018; Shi et al., 2016). Therefore, the modified path constraints with time-varying back-offs $\mathbf{b}_c(t) \geq \mathbf{0}$ read as:

$$\mathbf{h}(\mathbf{x}(t), \mathbf{z}(t), \mathbf{u}(t), \bar{\boldsymbol{\theta}}) + \mathbf{b}_c(t) \leq \mathbf{0}. \tag{16}$$

Next, the original path constraints (15) are replaced with Eq. (16) to give a modified dynamic optimization problem with time-varying back-offs as shown below:

$$\begin{aligned}\underset{\mathbf{x}(\cdot),\mathbf{u}(\cdot),\mathbf{z}(\cdot)}{\text{minimize}} \quad & \Phi(\mathbf{x}(t_\mathrm{f})) \\ \text{subject to} \quad & \dot{\mathbf{x}}(t) = \mathbf{f}(\mathbf{x}(t), \mathbf{z}(t), \mathbf{u}(t), \bar{\boldsymbol{\theta}}), \quad \forall t \in \mathcal{T}, \\ & \mathbf{g}(\mathbf{x}(t), \mathbf{z}(t), \mathbf{u}(t), \bar{\boldsymbol{\theta}}) = \mathbf{0}, \quad \forall t \in \mathcal{T}, \\ & \mathbf{h}(\mathbf{x}(t), \mathbf{z}(t), \mathbf{u}(t), \bar{\boldsymbol{\theta}}) + \mathbf{b}_c(t) \leq \mathbf{0}, \quad \forall t \in \mathcal{T}, \\ & \mathbf{x}(t_0) = \mathbf{x}_0, \\ & \mathbf{u}(t) \in \mathcal{U},\end{aligned} \tag{17}$$

on the time horizon $\mathcal{T} := [t_0, t_\mathrm{f}] \subset \mathbb{R}$.

Here, the subscript $c \in [0,\ 1]$ in the back-offs terms $\mathbf{b}_c(t)$ defines the confidence level of the robust solution as the probability that the jth inequality constraint h_j is satisfied in the presence of uncertainty, $c = \mathbb{P}[h_j(\mathbf{x}(t), \mathbf{z}(t), \mathbf{u}(t), \boldsymbol{\theta}) \leq 0]$. For example, a confidence level of $c = 0.99$ implies that the constraint h_j should be fulfilled for 99% of the scenarios.

Furthermore, we assume that back-off terms $\mathbf{b}_c(t)$ are insensitive to the decision variables (Shi et al., 2016). In our study, this assumption is justified as the back-off algorithm presented in Section 3.7 terminates after one iteration. Under this assumption, it has been proven by Shi et al. (2016) that the back-off formulation (17) is equivalent to a multi-scenario problem (Diehl et al., 2006) with the Karush-Kuhn-Tucker (KKT) conditions defined at a set of critical uncertainty points where path constraints are active. Please see Shi et al. (2016) for more details.

3.7. PEM-based back-off algorithm

The PEM-based back-off algorithm is presented in Algorithm 1. The main steps of the algorithm are explained as follows:

Algorithm 1: Back-off algorithm for robust optimization. (Reference (Schenkendorf, 2014) is cited in algorithm body part.)

Set counter $m = 0$ and $m_{\max}$
Initialize $\mathbf{b}_{c,\text{pem}}^{j,m} \longleftarrow \mathbf{0}$
Choose PEM points as described in Schenkendorf (2014)
Set n_p from Eq. (12)
Set η, $\epsilon_{\text{tol}}^{\Phi}$, $\epsilon_{\text{tol}}^{\text{rms}}$
Solve the nominal problem (10) at $\bar{\boldsymbol{\theta}}$ for $\mathbf{u}^*(t)$,$\mathbf{x}^*(t)$, $\mathbf{z}^*(t)$, $\Phi^*(t_f)$
Simulate $\dot{\mathbf{x}}(t) = \mathbf{f}(\mathbf{x}(t), \mathbf{z}(t), \mathbf{u}(t), \boldsymbol{\theta}_p), \quad \forall p \in \{1, \ldots, n_p\}$ with $\mathbf{x}^*(0)$, $\mathbf{u}^*(t)$
Update counter $m \longleftarrow m + 1$
Calculate $\mathbf{b}_{c,\text{pem}}^{j,m}$ with the nominal results
Calculate $\epsilon^{\text{rms}} \longleftarrow \frac{\|\mathbf{b}_{c,\text{pem}}^{j,m}(t) - \mathbf{b}_{c,\text{pem}}^{j,m-1}(t)\|}{\sqrt{|\mathcal{T}|}}$
Calculate $\mathbb{E}[\Phi(\mathbf{x}(t_f))]_m$
Set $\epsilon^{\Phi} \longleftarrow 1$
while $\epsilon^{\Phi} > \epsilon_{\text{tol}}^{\Phi}$ and $\epsilon^{\text{rms}} > \epsilon_{\text{tol}}^{\text{rms}}$ and $m < m_{\max}$ **do**
  Solve problem with back-offs (17) for $\mathbf{u}^*(t)$,$\mathbf{x}^*(t)$, $\mathbf{z}^*(t)$, $\Phi^*(t_f)$
  Simulate $\dot{\mathbf{x}}(t) = \mathbf{f}(\mathbf{x}(t), \mathbf{z}(t), \mathbf{u}(t), \boldsymbol{\theta}_p), \quad \forall p \in \{1, \ldots, n_p\}$ with $\mathbf{x}^*(0)$, $\mathbf{u}^*(t)$
  Update counter $m \longleftarrow m + 1$
  Calculate $\mathbf{b}_{c,\text{pem}}^{j,m}$ for the next iteration
  Calculate $\epsilon^{\text{rms}} \longleftarrow \frac{\|\mathbf{b}_{c,\text{pem}}^{j,m}(t) - \mathbf{b}_{c,\text{pem}}^{j,m-1}(t)\|}{\sqrt{|\mathcal{T}|}}$
  Calculate $\mathbb{E}[\Phi(\mathbf{x}(t_f))]_m$
  Calculate $\epsilon^{\Phi} \longleftarrow \frac{\mathbb{E}[\Phi(\mathbf{x}(t_f))]_m - \mathbb{E}[\Phi(\mathbf{x}(t_f))]_{m-1}}{\mathbb{E}[\Phi(\mathbf{x}(t_f))]_m}$
end while
Return $\mathbf{u}^*(t)$, $\mathbf{x}^*(t)$, $\Phi^*(t_f)$

1. First, the algorithm is initialized by setting the back-offs for constraint j at all collocation points in the finite elements to zero; i.e., $\mathbf{b}_{c,\text{pem}}^{j}(t) = 0$. The iteration counter is set to $m = 0$, and the maximum number of iterations $m_{\max}$ is set. The PEM points are selected as described in Section 3.5, the parameter η determining the confidence level is set, and the tolerances $\epsilon_{\text{tol}}^{\Phi}$ and $\epsilon_{\text{tol}}^{\text{rms}}$ for the convergence of the algorithm are set. We recommend setting both $\epsilon_{\text{tol}}^{\Phi}$ and $\epsilon_{\text{tol}}^{\text{rms}}$ to a default value of 10^{-2}.
2. Next, the nominal dynamic optimization problem (10) is solved at the nominal parameter point $\bar{\boldsymbol{\theta}}$ to obtain the nominal optimal controls $\mathbf{u}^*(t)$, states $\mathbf{x}^*(t)$, $\mathbf{z}^*(t)$, and the objective value $\Phi^*(t_f)$.
3. By using the nominal control trajectories and key decision variables, such as the initial condition, forward simulations of the system are performed for each PEM point to obtain different realizations.
4. Next, the time-varying back-offs are calculated based on the simulation results by using the following equations:

$$\mathbf{b}_{c,\text{pem}}^{j}(t) = \eta \times \sqrt{\text{Var}[\mathbf{h}_j(t)]} \tag{18}$$

$$\mathbb{E}[\mathbf{h}_j(t)] = w_0 \mathbf{h}_j(t, GF[0]) + w_1 \sum \mathbf{h}_j(t, GF[\pm\vartheta]) + w_2 \sum \mathbf{h}_j(t, GF[\pm\vartheta, \pm\vartheta]) \tag{19}$$

$$\begin{aligned}\text{Var}[\mathbf{h}_j(t)] = {} & w_0 (\mathbf{h}_j(t, GF[0]) - \mathbb{E}[\mathbf{h}_j(t)])^2 \\ & + w_1 \sum (\mathbf{h}_j(t, GF[\pm\vartheta]) - \mathbb{E}[\mathbf{h}_j(t)])^2 \\ & + w_2 \sum (\mathbf{h}_j(t, GF[\pm\vartheta, \pm\vartheta]) - \mathbb{E}[\mathbf{h}_j(t)])^2.\end{aligned} \tag{20}$$

   Note that the means and variances at each time point are approximated by using the PEM (cf. Section 3.5).
5. The dynamic optimization problem with the calculated time-varying back-offs is then solved (see Eq. (17)).
6. Next, the counter m is updated, and the difference between the back-offs of the constraint j at the current iteration $\mathbf{b}_{c,\text{pem}}^{j,m}$ and the previous iteration $\mathbf{b}_{c,\text{pem}}^{j,m-1}$ is checked by using the root-mean-square (RMS) prediction error ϵ^{rms}. These vectors (back-offs) are of the same dimension $|\mathcal{T}|$ which is equal to the number of time points at which the back-off values were calculated. In addition, the relative difference ϵ^{Φ} between the expected values of the objective at the current iteration and the previous iteration is determined.
7. Step 6 of the algorithm is repeated within a while loop until the convergence conditions $\epsilon^{\Phi} < \epsilon_{\text{tol}}^{\Phi}$ and $\epsilon^{\text{rms}} < \epsilon_{\text{tol}}^{\text{rms}}$ are satisfied or the maximum number of iteration $m_{\max}$ is reached, and the algorithm terminates.
8. Lastly, the robust optimal controls and states are obtained and validated with the Monte Carlo-based back-off approach as presented in Section 3.8.

3.8. Assessment of estimation accuracy

To assess the accuracy of the back-offs calculated by using the PEM, we also run the back-off algorithm by using Monte Carlo simulations to calculate the means and variances. Here, we use Monte Carlo simulations as a benchmark for the PEM as they are assumed to lead to more accurate estimates of the statistical moments due to the *weak law of large numbers* (Bertsekas and Tsitsiklis, 2008).

The only difference between the PEM-based back-off algorithm and the Monte Carlo-based back-off algorithm lies in the way that the statistical moments are calculated. In the case of the Monte Carlo approach, the mean and variance of the jth inequality constraint are given by the following natural estimators:

$$\mathbb{E}[\mathbf{h}_j(t)] = \frac{\sum_{i=1}^{N} \mathbf{h}_j(\mathbf{x}(t), \mathbf{z}(t), \mathbf{u}(t), \bar{\boldsymbol{\theta}})}{N}, \tag{21}$$

$$\text{Var}[\mathbf{h}_j(t)] = \frac{\sum_{i=1}^{N} (\mathbf{h}_j(\mathbf{x}(t), \mathbf{z}(t), \mathbf{u}(t), \bar{\boldsymbol{\theta}}) - \mathbb{E}[\mathbf{h}_j(t)])^2}{N - 1}, \tag{22}$$

where N is the number of Monte Carlo samples.

Next, we compare the PEM-based back-offs to the Monte Carlo-based back-offs by using the RMS prediction error (Boyd and Vandenberghe, 2018):

$$\mathbf{rms}(\mathbf{b}_{c,\text{mc}}^{j}(t) - \mathbf{b}_{c,\text{pem}}^{j}(t)) = \frac{\|\mathbf{b}_{c,\text{mc}}^{j}(t) - \mathbf{b}_{c,\text{pem}}^{j}(t)\|}{\sqrt{|\mathcal{T}|}}, \tag{23}$$

where $\mathbf{b}_{c,\text{mc}}^{j}$ and $\mathbf{b}_{c,\text{pem}}^{j}$ are the time-varying back-offs of the constraint j calculated from the Monte Carlo simulations and the PEM, respectively, and $\|\cdot\|$ refers to the Euclidean norm.

3.9. Implementation

The nominal and robust dynamic optimization problems were implemented in the Matlab API for CasADi 3.4.0, a framework for automatic differentiation and numerical optimization (Andersson et al., 2018). Furthermore, 50 finite elements and 3 Radau collocation points were used to discretize the dynamic optimization problems as described in Section 3.3.

The resulting NLPs were solved by using the interior point NLP solver IPOPT (Wächter and Biegler, 2006) with the MA57 linear solver (Duff, 2004) from the Harwell Subroutine Library (HSL, 2007). The sparsity patterns of Hessian and Jacobian matrices are shown in Appendix B (cf. Fig. B.2). The sparsity and

structure of these matrices are advantageous as the IPOPT algorithm is able to exploit this sparsity to solve the NLP faster. All computations were performed on a UNIX-based laptop with a 2.7 GHz Intel Core i5 processor and 8 GB RAM.

4. Optimization strategies for *Pf*BAL-catalyzed carboligation without uncertainties

In this section, we present the optimization formulation and results for the case study considered without uncertainties. That is, we analyze the nominal problem first.

4.1. Model formulation

To mathematically formulate the fluid element that is to be tracked as explained in Section 3.1, mole balances for components A, B, BA, BB, and E are required. For this study, we transform the mass balances from the regular EPF molar basis which is based on intensive properties to a concentration basis as follows:

$$\dot{\mathbf{x}}(t) = \mathbf{f}_{\text{epf}}(\mathbf{x}(t), \mathbf{z}(t), \mathbf{u}(t), \boldsymbol{\theta}) = \begin{bmatrix} \frac{j_A}{V} - \frac{C_A}{V}(u_A + u_B) + r_A \\ \frac{j_B}{V} - \frac{C_B}{V}(u_A + u_B) + r_B \\ -\frac{C_{BA}}{V}(u_A + u_B) + r_{BA} \\ -\frac{C_{BB}}{V}(u_A + u_B) + r_{BB} \\ -\frac{C_E}{V}(u_A + u_B) + r_E \\ u_A + u_B \end{bmatrix}, \tag{24}$$

with

$$j_A = u_A \cdot C_A^{\text{in}}, \tag{25}$$

$$j_B = u_B \cdot C_B^{\text{in}}. \tag{26}$$

We perform this transformation to ensure the proper and consistent representation of the path constraints which will be shown in the next section. The proper representation of these path constraints is important because a major aim of this work is to ensure that they are not violated due to parametric uncertainty.

Eq. (24) in combination with the rate Eqs. (1)–(5) leads to a semi-explicit differential-algebraic equation (DAE) system, where the state vector is given as $\mathbf{x}(t) := [C_A, C_B, C_{BA}, C_{BB}, C_E, V]^\top$, with C_i denoting the concentration of species i. The controls are given as $\mathbf{u}(t) := [u_A, u_B]^\top$, where u_A and u_B represent the volumetric flow rates of A and B, respectively; and $\mathbf{z}(t) := [r_A, r_B, r_{BA}, r_{BB}, r_E]^\top$ is a vector of the algebraic variables. C_A^{in} and C_B^{in} are the inlet feed concentrations of propanal and benzaldehyde, respectively. The inlet feed concentrations of propanal and benzaldehyde are assumed to be pure and are calculated as $C_A^{\text{in}} = \frac{1000 \times 810}{58.08}$ mmol^{-1}L and $C_B^{\text{in}} = \frac{1000 \times 1040}{106.121}$ mmol^{-1}L, respectively.

4.2. Dynamic optimization formulation

The aim of the nominal dynamic optimization problem is to maximize the final concentration of the product BA by optimizing the flow rates u_A and u_B, the initial conditions. Thus, the problem-specific dynamic optimization formulation is given as:

$$\underset{\substack{u_A(t),\ u_B(t),\ C_{A,0},\\ C_{B,0},\ C_{E,0},\ V_0}}{\text{minimize}} \quad -C_{BA}(t_f) \tag{27a}$$

$$\text{subject to } \dot{\mathbf{x}}(t) = \mathbf{f}_{\text{epf}}(\mathbf{x}(t), \mathbf{z}(t), \mathbf{u}(t), \bar{\boldsymbol{\theta}}), \quad \forall t \in [0, t_f] \tag{27b}$$

$$0 \le \mathbf{x}_0 \le \mathbf{x}_0^{\text{U}} \tag{27c}$$

Table 2
Upper bounds for the nominal dynamic optimization problem.

Symbol	Value	Unit
$C_{A,0}^{U}$	100	mmol^{-1}L
$C_{B,0}^{U}$	149.35	mmol^{-1}L
$C_{BA,0}^{U}$	0	mmol^{-1}L
$C_{BB,0}^{U}$	0	mmol^{-1}L
$C_{E,0}^{U}$	50	mmol^{-1}L
C_{A}^{U}	100	mmol^{-1}L
C_{B}^{U}	149.35	mmol^{-1}L
C_{BA}^{U}	10,000	mmol^{-1}L
C_{BB}^{U}	2.78	mmol^{-1}L
C_{E}^{U}	50	μg^{-1}mL
t_f	300	min

$$0 \le \mathbf{x}(t) \le \mathbf{x}^{\text{U}}, \quad \forall t \in [0, t_f] \tag{27d}$$

$$0 \le \mathbf{u}(t) \le \mathbf{u}^{\text{U}}, \quad \forall t \in [0, t_f]. \tag{27e}$$

Note that in addition to the controls u_A and u_B, the initial conditions of the states $\mathbf{x}_0$ such as the initial volume and concentrations of species i are also considered decision variables. However, the initial concentrations of the products $C_{BA,0}$ and $C_{BB,0}$ are constrained to zero since we assume that no product is present at the onset of the reaction. As a result, $C_{BA,0}$ and $C_{BB,0}$ are eliminated as decision variables. Furthermore, $\mathbf{x}_0^{\text{U}} := [C_{A,0}^{U}, C_{B,0}^{U}, C_{BA,0}^{U}, C_{BB,0}^{U}, C_{E,0}^{U}, V_0^{U}]^\top$ is a vector containing the upper bounds for the initial conditions of the states, and the upper bound for the state vector is defined as $\mathbf{x}^{\text{U}} := [C_A^{U}, C_B^{U}, C_{BA}^{U}, C_{BB}^{U}, C_E^{U}, V^{U}]^\top$. The actual values of $\mathbf{x}_0^{\text{U}}$ and $\mathbf{x}^{\text{U}}$ are stated in Table 2. Please, note that the upper bounds for A, B, and E at the initial conditions and during the operation are the same. The upper bounds for B and BB were set to their solubility limits to avoid issues with clogging (Hartman, 2012). The bounds for A and E are ranges at which the kinetic experiments where performed – this is to ensure that the reaction kinetics remain valid during the optimization procedure. Finally, t_f was fixed to 300 min to avoid quenching the reaction before the enzyme was properly inactivated. This is important because the presence of enzyme facilitates the production of BA.

4.3. Intensification cases

In this work, different intensification cases were investigated to ascertain the best case for the maximization of the final concentration of (*R*)-2-hydroxy-1-phenylbutan-1-one (BA) produced by the *Pf*BAL-catalyzed carboligation between propanal (A) and benzaldehyde (B). First, a reference case is presented to benchmark the performance of the other intensification cases on it. To this end, a batch reactor was selected because it is the most common reactor used for enzyme-catalyzed reactions. Three intensification cases were considered systematically and are described in more detail below.

Case 1: Dosing of propanal. In this case, the possibility of dosing only propanal (A) during the course of the reaction was considered to see if it leads to improvements in the final concentration of BA in comparison to the reference batch reactor. Here, the dosing (volumetric) flux of A u_A in Eq. (24) was dynamically optimized and the dosing flux of B was set to zero ($u_B = 0$). In addition to u_A, $C_{A,0}$, $C_{B,0}$, $C_{E,0}$ and V_0 required for the highest possible concentration of BA were also determined.

Table 3
Optimal initial reactant concentrations $C_{A,0}$ and $C_{B,0}$, optimal initial enzyme concentration $C_{E,0}$ and maximum final product concentration $C_{BA}(t_f)$ of each intensification case considered.

Case	$C_{A,0}$ [mmol^{-1}L]	$C_{B,0}$ [mmol^{-1}L]	$C_{E,0}$ [μg^{-1}mL]	$C_{BA}(t_f)$ [mmol^{-1}L]
Reference (batch)	11.16	6.61	50	3.11
Case 1	3.65	6.51	50	3.18
Case 2	11.94	1.92	50	3.52
Case 3	0.83	3.09	50	3.60

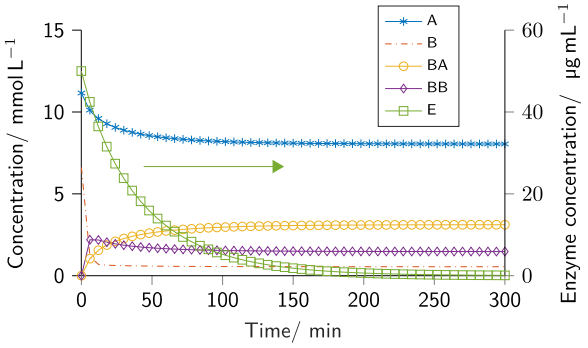

Fig. 4. Nominal dynamic optimization results for the reference batch reactor case: concentration profiles.

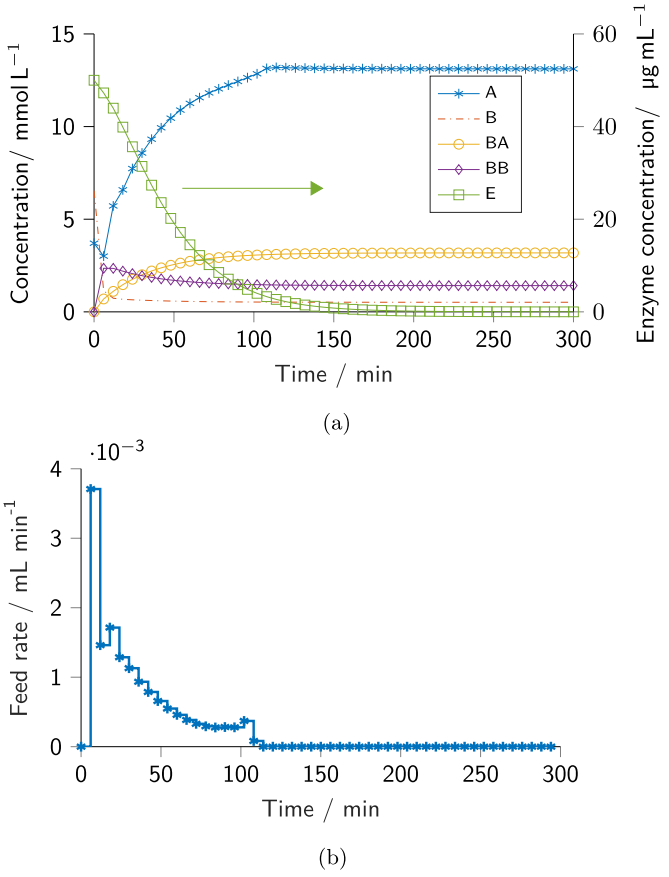

Fig. 5. Nominal dynamic optimization results for the intensification case 1 involving the dosing of propanal. Concentration profiles (states) (a); Feed rate of propanal as a control (b).

Case 2: Dosing of benzaldehyde. Similar to case 1, the possibility of dosing only benzaldehyde (B) along the reaction coordinate was investigated. Here, u_B, $C_{A,0}$, $C_{B,0}$, $C_{E,0}$ and V_0 were optimized with the goal of maximizing the final concentration of the target product BA.

Case 3: Dosing of propanal and benzaldehyde. This case marks the most flexible setting where all tunable operating conditions are optimized to maximize the concentration of BA. In concrete terms, the dynamic dosing fluxes of reactants A and B (u_A and u_B) were optimized to investigate possible interactions between the reactants. Similar to cases 1 and 2, $C_{A,0}$, $C_{B,0}$, $C_{E,0}$ and V_0 were also optimized.

4.4. Selecting the best intensification case

In the following, we discuss and compare the nominal dynamic optimization results for the various intensification cases. The optimal decision variables and the maximum final concentration of BA for each intensification case are presented in Table 3, while the concentration and optimal control profiles are shown subsequently.

4.4.1. Results for the reference case: Batch reactor

We focus on the concentration profiles of the batch reactor as shown in Fig. 4. For this case, the final concentration of the target product BA is 3.11 mmol L^{-1} (see Table 3). Here, propanal (A) starts at a concentration of 11.16 mmol L^{-1} and then decreases gradually to 8.05 mmol L^{-1}. Concurrently, benzaldehyde (B) starts at 6.61 mmol L^{-1} and decreases at a faster rate in comparison to reactant A to 0.55 mmol L^{-1}. It can be seen that the optimal initial concentration of A is higher than that of B. This is logical as the rate equations and molar balances reveal a proportional relationship between reactant A and the target product BA. First, every consumption of A leads to a formation of AB. Therefore, a high A concentration maximizes AB. As B may also form BB, its rate of consumption is faster than for A. However, to minimize losses to BB, a lower concentration of B is chosen. This can also be seen in the reaction scheme 1 and in the rate equations.

Furthermore, the enzyme concentration starts at the upper bound of 50 μg^{-1}mL to produce BA as fast as possible and gradually decreases to zero at about 200 min signifying the inactivation of the enzyme. After this point, it can be seen in Fig. 4 that the concentration of BA and BB reaches steady state. Another key observation is that the concentration of BA is almost maximized after the enzyme inactivates. This is due to two reasons. First, the benzaldehyde self-carboligation step appears to have reached an equilibrium, and the inactivity of the enzyme implies that the cross-carboligation reaction to produce BA is inhibited.

4.4.2. Results for case 1: dosing of propanal

With the results of the batch case delineated, we now discuss the effect of dosing only propanal (A) along the reaction route as shown in Fig. 5. By dosing A, the final concentration of (*R*)-2-hydroxy-1-phenylbutan-1-one (BA) achieved is 3.18 mmol L^{-1} (cf. Table 3). This is a marginal improvement of 2.25% over the reference batch case. In Fig. 5, we observe a non-intuitive concentration profile in comparison to the results of the batch reactor reference case. Here, reactant A starts at a concentration of 3.65 mmol L^{-1} which is lower than the initial concentration of B in this case. The initial concentration of B is 6.51 mmol L^{-1} which is very similar to that of the reference case.

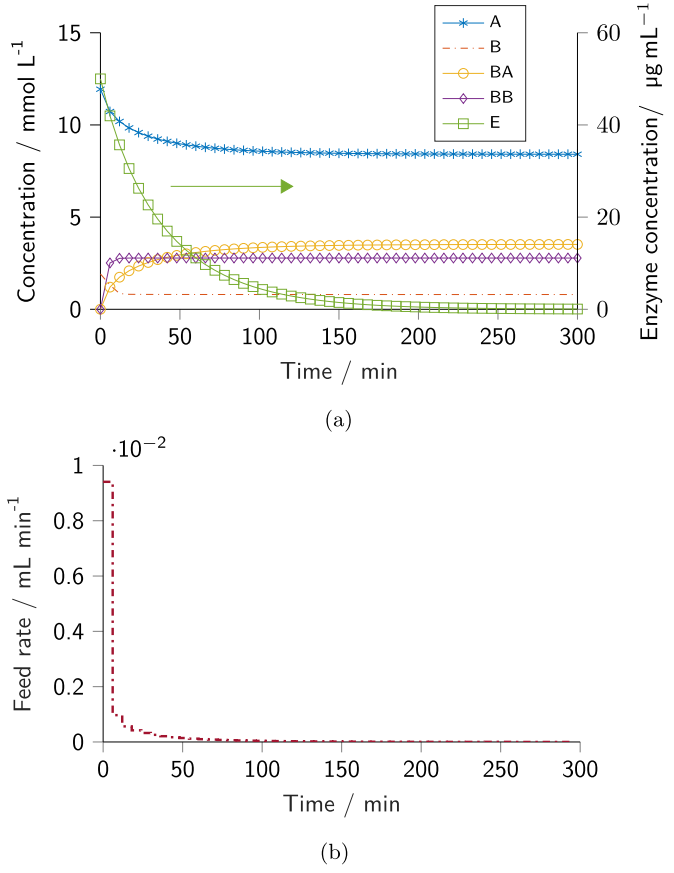

Fig. 6. Nominal dynamic optimization results for the intensification case 2 involving the dosing of benzaldehyde. Concentration profiles (states) (a); Feed rate of benzaldehyde as a control (b).

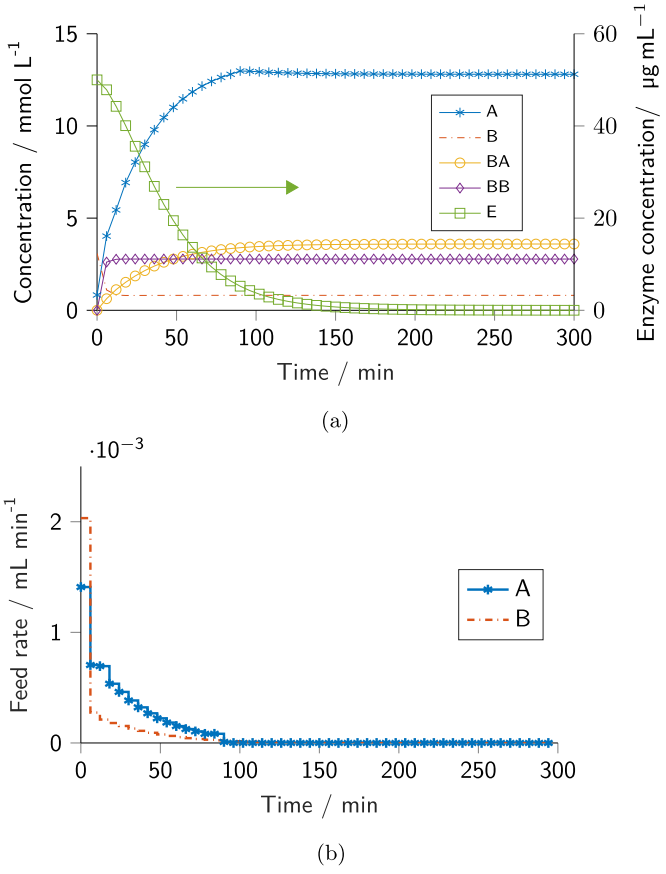

Fig. 7. Nominal dynamic optimization results for the intensification case 3 involving the dosing of propanal and benzaldehyde. Concentration profiles (states) (a); Feed rates of propanal (A) and benzaldehyde (B) as controls (b).

However, we notice that the concentration of A decreases to 2.96 mmol L^{-1} after 6 min at which point the product BB is maximized. Afterward, the dosing of A is initiated, thus leading to an increase in the concentration of reactant A during the reaction. This is a non-intuitive strategy that requires some more explanation. First, reactant A has to be started at a lower concentration in this case because the optimizer recognized that dosing A would be required after 6 min to maximize the formation of BA. However, starting A at a higher concentration similar to that of the reference case might lead to faster inactivation of the enzyme and thus a lower final product. As a result, the optimizer detects 3.65 mmol L^{-1} as the optimal initial concentration for B.

With regards to the decrease in A in the first 6 min, it can be observed that this increase coincides with the maximum concentration of the side product BB (at 2.36 mmol L^{-1}). Afterwards, BB starts to decrease due to a reverse reaction as illustrated in Fig. 1. This leads to a "domino effect" in which the reverse reaction to produce B is triggered to ensure that sufficient B is maintained in the reaction medium to react with A to produce BA.

Consequently, the concentration of A is increased by dosing A so that it can continuously react with the almost constant concentration of B to produce as much BA as fast as possible. Similar to the reference case, we notice that the reaction between A and B is halted and that the concentration of BA reaches a constant value as soon as the enzyme is inactivated. For similar reasons, the inactivation of the enzyme implies that the reaction between A and B can no longer be catalyzed and thus, the formation of BA stops. We also notice that the feeding of A stops at the same time the enzyme is inactivated. This is obviously rational as there is no need to keep feeding propanal (A) if the enzyme is not active to catalyze its reaction benzaldehyde (B). Unfortunately, dosing A adversely affects the enzyme activity, i.e., the enzyme inactivates after approximately 138 min of reaction which is shorter than the time (about 180 min) it takes for the enzyme to inactivate for the reference case. Overall, the final concentration of BA is slightly improved by dosing propanal.

4.4.3. Results for case 2: Dosing of benzaldehyde

As seen in Fig. 6(a), the case of dosing only benzaldehyde (B) yields similar concentration profiles like the reference case. The optimal initial concentrations of A and B are 11.94 and 1.92 mmol L^{-1}, respectively. By dosing only B, the final BA concentration of 3.52 mmol L^{-1} is achieved (cf. Table 3). This results in a 13.18% increase over the reference case. It can be seen that it is more advantageous to dose B in comparison to A. The reason for this increase in comparison to the reference case and the case in which only A was dosed is primarily due to the optimal selection of the initial concentration and the dosing trajectories of B.

In this case, the optimal initial concentration of B is approximately three times lower than those in the batch reference and the intensification case 1, i.e., dosing of propanal. Here, the rate at which BB is formed is kept lower than the two previous cases by ensuring that a lower amount of B is allowed to bind to the enzyme. Despite this lower concentration, an appropriate amount of B which ultimately leads to the maximization of $C_{BA}(t_f)$ is ensured by an optimal feed rate that starts high and gradually decreases

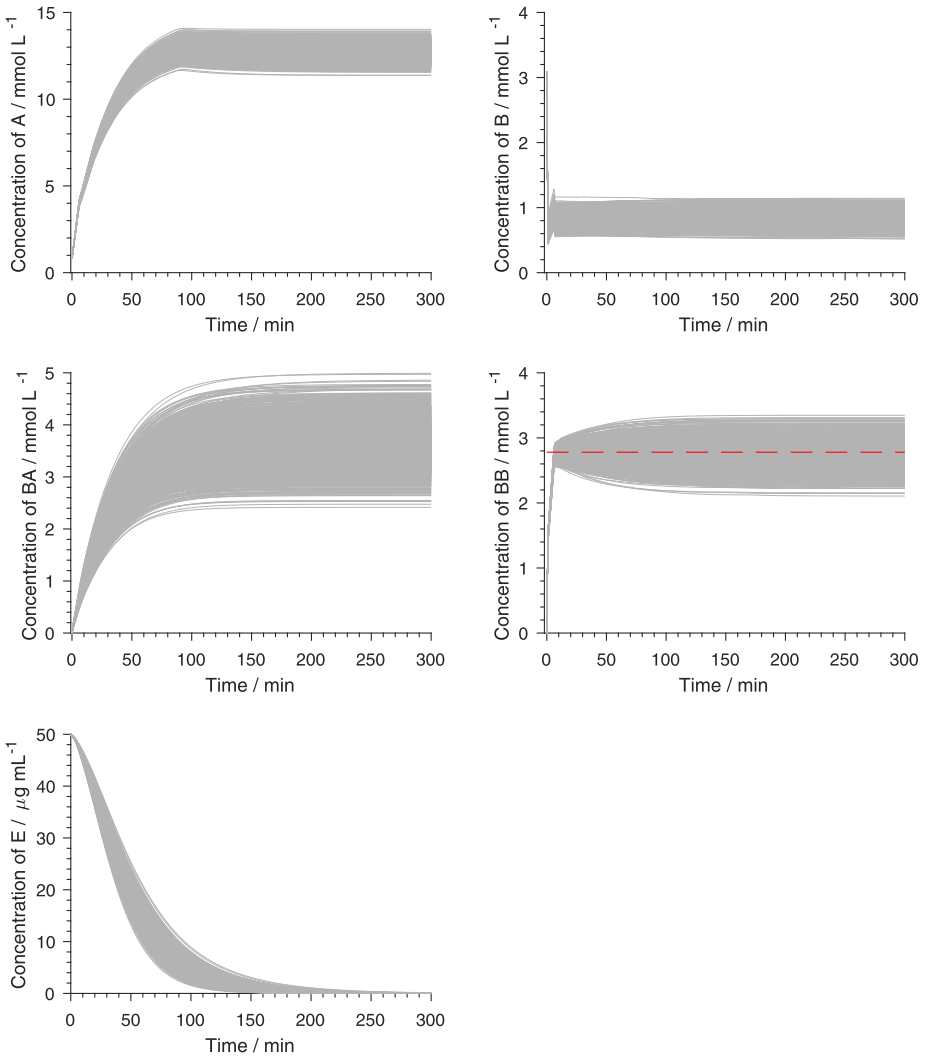

Fig. 8. Concentrations for 2000 forward Monte Carlo simulations using the nominal control profiles for the case of dosing A and B (i.e. case 3). The dotted red line is the solubility constraint for BB, and the gray lines the 2000 Monte Carlo simulations. (For interpretation of the references to colour in this figure legend, the reader is referred to the web version of this article.)

along the reaction coordinate (cf. Fig. 6(b)). Furthermore, the lower amount of B present during the reaction ensures that the rate of enzyme inactivation due to B is slower. Consequently, the presence of a slightly higher concentration of the enzyme during the reaction leads to the higher concentration of BA.

4.4.4. Results for case 3: Dosing of propanal and benzaldehyde

The nominal optimization results for the case in which A and B are dosed simultaneously are shown in Fig. 7. Here, the optimal initial concentrations of A and B are 0.83 and 3.09 mmol L^{-1}, respectively. It can be observed that the simultaneous dosing of A and B is akin to the superposition of the results of dosing A and B alone. Therefore, the reasons behind the previous results also apply here.

Furthermore, the enzyme concentration starts at the upper bound of 50 μg^{-1}mL for similar reasons as previously discussed. In addition, the concentration of BB eventually hits its maximum value at the end of the reaction time to ensure that BA is maximized.

Moreover, by dosing A and B, the final concentration of BA obtained is 3.60 mmol L^{-1} (see Table 3). This is the highest final concentration of BA obtained among all the intensification cases considered, i.e., a 15.76% increase over the reference case. This increase

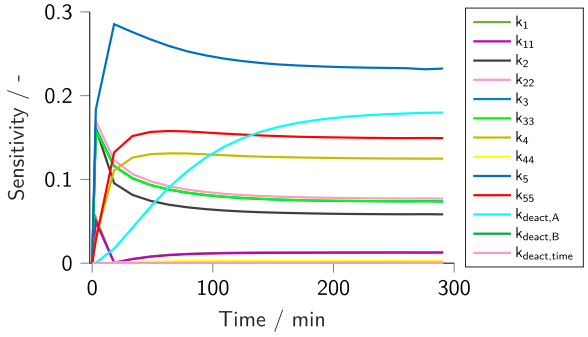

Fig. 9. Sensitivity results of 13 model parameters for the concentration of BB. (For interpretation of the references to colour in this figure legend, the reader is referred to the web version of this article.)

can be attributed more to the dosing of B only as it is very close to the value of $C_{BA}(t_f)$ obtained when only B was dosed.

Nevertheless, dosing A and B simultaneously ensures that the highest possible final concentration of BA is obtained since the benefits of dosing A and B are fully exploited. Therefore, this case is selected for robustification in the subsequent sections.

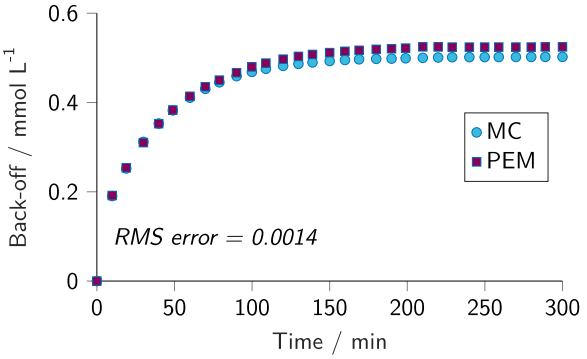

Fig. 10. Comparison of time-varying back-offs for the constraint $C_{BB}(t) - 2.78 \leq 0$ calculated with the point estimate method (PEM) with those calculated with Monte Carlo (MC) simulations. RMS error stands for the root-mean-square prediction error.

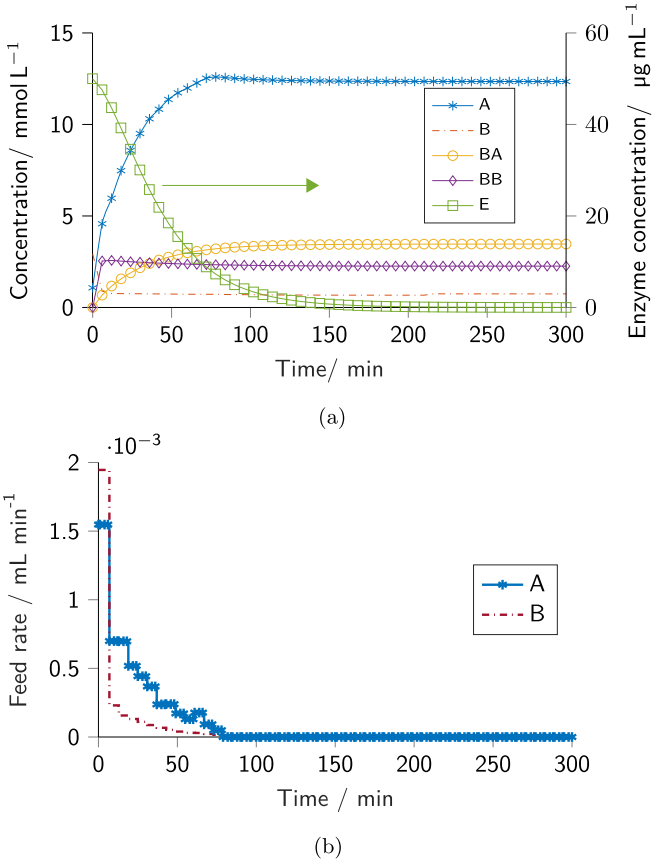

Fig. 11. Robust dynamic optimization results for the intensification case 3 involving the dosing of propanal and benzaldehyde. Concentration profiles by using the robust control at the nominal parameter point (a); Robust feeding profiles (controls) for propanal (A) and benzaldehyde (B) (b).

5. Optimization of *Pf*BAL-catalyzed carboligation under uncertainties

5.1. Forward uncertainty propagation with nominal controls

In a first step, we performed 2000 Monte Carlo simulations with the initial conditions and flow rates (controls) of the best intensification case in which propanal and benzaldehyde were both dosed. Here, we found that 2000 Monte Carlo simulations were

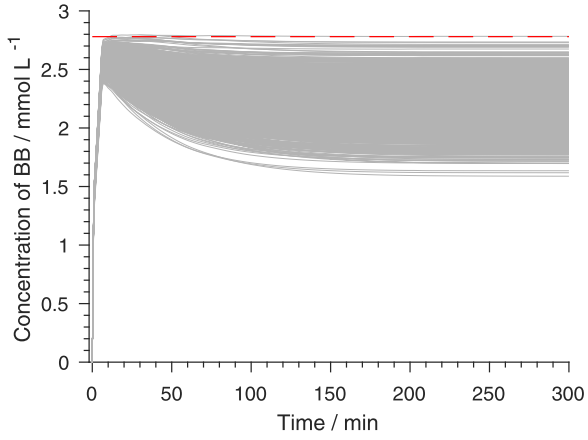

Fig. 12. Verification of the robust control considering all parameters with 2000 Monte Carlo samples. The dotted red line is the solubility constraint for BB, and the grey lines the 2000 Monte Carlo simulation results. (For interpretation of the references to colour in this figure legend, the reader is referred to the web version of this article.)

sufficient for estimating the statistical moments. As described in Section 3, Monte Carlo simulations were performed to determine if the nominal controls led to violations of the upper bounds (see Table 2) in the presence of parametric uncertainty. If any of the upper bounds are violated then the subsequent robustification steps (cf. Fig. 2) are performed, else the nominal control is sufficient for operating the process. As we can see in Fig. 8, all the states are within their upper bounds except for the concentration of benzoin C_{BB} where the constraint was violated 56.95% of the time. As only C_{BB} was violated, we then focus on robustifying C_{BB} by using the PEM-based back-off algorithm described in Section 3.6.

5.2. Determining the sensitive parameters

For the sensitivity analysis, the parameters are assigned normal distributions with a mean equal to their nominal values and a standard deviation equal to 10% of their nominal values. Results of the first-order sensitivity indices at different time points for the concentration of BB are given in Fig. 9. Please note that the sensitivity study revealed negligible parameter interactions, i.e., the values of total sensitivity indices are similar to those of the first-order sensitivity indices, and thus, are not shown here. Also note that the sensitivity analysis was performed on the reference (batch reactor) case described in Section 4.3.

As we can observe from the figure, the majority of parameter uncertainties have a distinct impact on the quantity we are interested in, i.e., the concentration of BB. However, the sensitivities for uncertainties of the parameters k_{44}, $k_{\text{deact, B}}$ and $k_{\text{deact, time}}$ are barely visible, and thus, their impact can be neglected to further reduce the complexity of our problem. In other words, only the uncertainties of the remaining 10 parameters were taken into account in the following calculations. This is important because it reduces the original number of PEM points from $2 \times 13^2 + 1 = 339$ to 201 points – a 40.71% reduction in the number of PEM points.

Uncertainties in other quantities, i.e., concentrations of A, B, BA, and E do not affect the result of the robust optimization, and their sensitivity results are shown in the Appendix (see Fig. A.1) for the sake of completeness.

5.3. Robust dynamic optimization formulation

By applying the robust optimization strategy presented in Section 3.6, the back-off dynamic optimization formulation for the

*Pf*BAL-catalyzed reaction reads as:

$$\underset{\substack{u_A(t),\ u_B(t),\ C_{A,0},\\ C_{B,0},\ C_{E,0},\ V_0}}{\text{minimize}} \quad -C_{BA}(t_f) \tag{28a}$$

$$\text{subject to } \dot{\mathbf{x}}(t) = \mathbf{f}_{epf}(\mathbf{x}(t), \mathbf{z}(t), \mathbf{u}(t), \bar{\boldsymbol{\theta}}), \quad \forall t \in [0, t_f] \tag{28b}$$

$$0 \leq \mathbf{x}_0 \leq \mathbf{x}_0^U \tag{28c}$$

$$0 \leq C_{BB}(t) \leq C_{BB}^U - b_c(t), \quad \forall t \in [0, t_f] \tag{28d}$$

$$0 \leq C_i(t) \leq C_i^U, \quad \forall i \in \{A, B, BA, E\}, \quad \forall t \in [0, t_f] \tag{28e}$$

$$0 \leq \mathbf{u}(t) \leq \mathbf{u}^U, \quad \forall t \in [0, t_f]. \tag{28f}$$

Note that time-varying back-offs are assigned only to the inequality constraint for C_{BB} in problem (28). The reason for this stems from the results of the forward simulations in Section 5.1 which show that only C_{BB} violates its solubility bound and should, therefore, be robustified. The confidence level c for the back-offs $b_c(t)$ in Eq. (28d) was set to 99.90% by choosing $\eta = 3$ in the back-off algorithm. The tolerances ϵ_{tol}^{Φ} and ϵ_{tol}^{rms} required for Algorithm 1 to converge were both set to 10^{-2}.

To apply the back-off algorithm, only the 10 parameters identified by the sensitivity analysis to be critical are considered uncertain. These 10 parameters are assigned normal distributions with a mean equal to their nominal values and a standard deviation equal to 10% of their nominal values. The remaining 3 parameters are considered certain and are fixed to their nominal values (cf. Table 1).

5.4. Robust optimization results

We now report the robust optimization results obtained by using the proposed PEM-based back-off algorithm. First, we investigate the accuracy of the PEM in calculating the time-varying back-offs by comparing with the back-offs calculated by Monte Carlo simulations. As shown in Fig. 10, the back-off increases with time for both cases; this is attributed to increasing BB concentrations with time, and as such to a decrease in distance to the solubility bound C_{BB}^U. As soon as self-carboligation stops towards the end of the reaction, the back-offs stabilize.

Nevertheless, the back-offs calculated with the PEM are approximately equal to those calculated by Monte Carlo simulations from 0 to 80 min of the reaction time (cf. Fig. 10). After 80 min, we observe that the back-offs calculated by the PEM gradually become slightly higher than those calculated by Monte Carlo simulations as time progresses. This suggests that the PEM-based back-off strategy could lead to a slightly more conservative robust design in comparison to a Monte Carlo-based back-off strategy. Another reason for this is because higher back-offs imply higher margins from the solubility limits (path constraints) and a smaller feasible region. Nevertheless, the results show that the back-offs calculated by the PEM are in general very close to those calculated by Monte Carlo simulations (cf. Fig. 10). This is further justified by the very small RMS prediction error of 0.0014 as shown in Fig. 10.

Fig. 11(b) shows the robust feed rates (controls) for the best intensification case. On a closer look at the robust controls, we see that it follows a similar control sequence like the nominal control (cf. Fig. 7(b)) with some subtle differences. First, the robust propanal (A) control starts at 1.55 mL min^{-1} while the nominal control of A starts lower at approximately 1.41 mL min^{-1}. In addition, the robust control sequence for A is coarser than its nominal counterpart within the first 80-min interval. In contrast, the only major difference between the robust and nominal controls for benzaldehyde (B) is that the robust B control starts at 1.95 mL min^{-1} while its nominal counterpart starts at 2.0 mL min^{-1}.

In addition to the robust controls, our preliminary studies revealed that the initial concentrations of reactants A and B are crucial in ensuring that a feasible solution is obtained for either the nominal or the robust optimization case. As a result, the initial conditions for the reactants and the enzyme were left as decision variables as described in Section 4.2. In Fig. 11(a), the concentration profiles obtained by using the robust control at the nominal parameter point have the following optimal initial concentrations: 1.07 mmol L^{-1}, 2.93 mmol^{-1}L and 50 µg mL^{-1} for A, B, and E, respectively. In addition, these robust controls lead to a BA final concentration of 3.47 mmol L^{-1} while ensuring that 99.90% of the 2000 Monte Carlo simulations are within the solubility limit of BB as shown in Fig. 12. However, this comes at the expense of $C_{BA}(t_f)$ which is 3.61% lower than that obtained for the nominal case as shown in Section 4.4.4 and Table 4.

Table 4
Comparison of the performance of the point estimate method-based (Robust-PEM) with the Monte Carlo-based (Robust-MC) back off algorithm for robust dynamic optimization.

	$C_{BA}(t_f)$ [mmol^{-1}L]	ϵ^{viol} [%]	CPU time [s]
Nominal	3.60	59.56	4
Robust-PEM	3.47	0.10	66
Robust-MC	3.46	0.15	714

$C_{BA}(t_f)$ means the final concentration of BA which is the objective function. ϵ^{viol} means the percentage of constraint violations.

As a benchmark, we compared the robust optimization results obtained by using the PEM-based back-off strategy to the Monte Carlo-based back-off algorithm presented in Koller et al. (2018). As we can see in Table 4, the 0.10% constraint violation obtained with our PEM back-off algorithm is very close to the 0.15% constraint violation obtained by using the Monte Carlo-based back-off algorithm. Furthermore, we observe that the final concentrations of BA for the two approaches are almost equal (cf. Table 4).

Moreover, using the PEM for the back-off is considerably faster than using Monte Carlo simulations. Specifically, the PEM-based robust optimization has a CPU time of 66 s while the Monte Carlo-based back-off algorithm takes approximately 714 s. Therefore, the PEM-based algorithm is approximately 11 times faster than the Monte Carlo-based algorithm for the application considered. This speed-up is mainly due to the lower number of PEM sample points ($2 \times 10^2 + 1 = 201$) in comparison to the 2000 Monte Carlo sample points. These results demonstrate that the PEM-based back-off strategy is very efficient and useful for the enzyme-catalyzed carboligation considered in this work.

6. Conclusions

A new framework for the robust optimization of enzyme-catalyzed carboligations was presented. The framework ensures that the best intensification case is selected by using the elementary process functions approach and that only critical parameters are considered in the robust optimization step by applying global sensitivity analysis. Specifically, dosing both propanal and benzaldehyde is predicted to lead to a 15% increase in the final concentration of (*R*)-2-hydroxy-1-phenylbutan-1-one when compared to a reference batch reactor.

Moreover, a key component of the proposed robust optimization approach is a new point estimate-based back-off algorithm

which is shown to be at least an order of magnitude faster than the conventional Monte Carlo-based back-off algorithm. Although the proposed approach does not consider the mean-variance formulation as is typically done in robust optimization, we have shown that the point estimate-based back-off algorithm effectively robustifies the reactor design, while ensuring a relatively high concentration of BA under parametric uncertainties.

Another important advantage of our approach is that the dynamic optimization problem(s) within the back-off algorithm can be solved with the same computational complexity as the nominal case. In our experience, this is easier and more computationally tractable to solve than conventional robust optimization formulations with chance constraints. Therefore, this implies that the approach presented in this paper could be easily extended to larger models involving whole (pharmaceutical) process chains. Besides the enzyme-catalyzed carboligation considered in this paper, the proposed robust optimization approach could be applied to other pharmaceutical processes (and even non-pharmaceutical processes) to ensure Quality by Design (QbD) standards.

Acknowledgments

We acknowledge and thank Florian Baakes for his preliminary work. Author Xiangzhong Xie acknowledges funding from the "Promotionsprogramm μ-Props" by MWK Niedersachsen.

Appendix A. Further sensitivity analysis results

Here, further sensitivity analysis results for components A, B, BA and E are presented. The first-order sensitivity indices are plotted in Fig. A.1. It can be observed that the sensitivity results for the concentrations of A and BA are identical. This is because their concentrations are directly correlated with a 1:1 ratio as shown in the reaction scheme (see Fig. 1). In addition, the sensitivity result for enzyme E is quite different from that for the other components. This is because the reaction rate of E is directly connected to the inactivation coefficients, and the concentration of A for the entire reaction period is larger than 1 and much higher than that of concentration B. Therefore, the inactivation coefficient $k_{\text{deact, A}}$ dominates the variation in the concentration of component E.

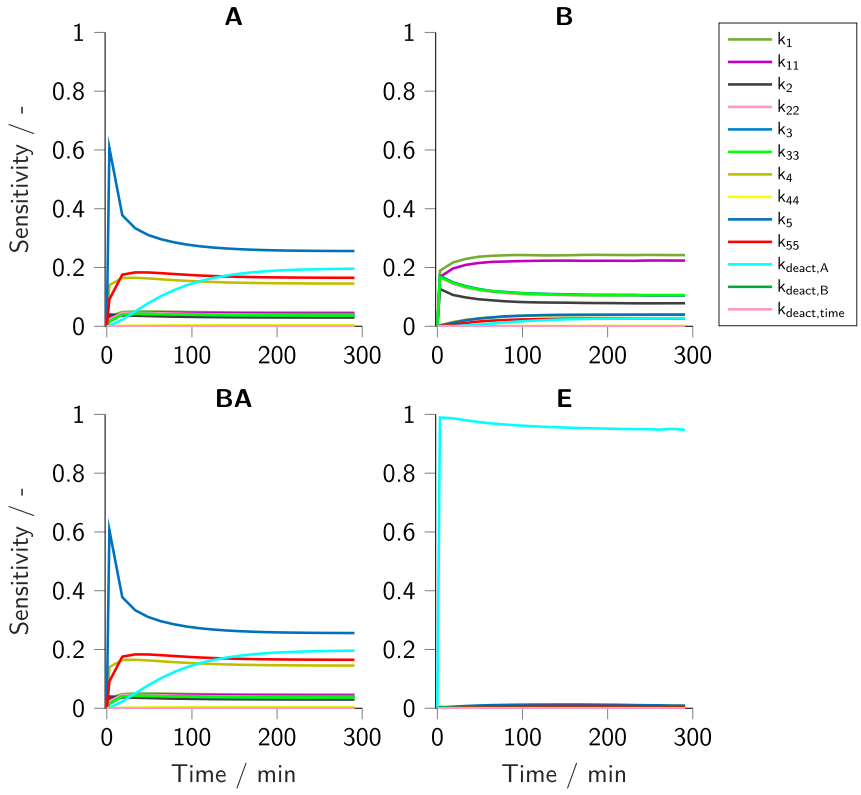

Fig. A1. Sensitivity results of 13 model parameters for the active constraints, i.e., concentrations of A, B, BA and E. (For interpretation of the references to colour in this figure legend, the reader is referred to the web version of this article.)

Appendix B. Sparsity patterns

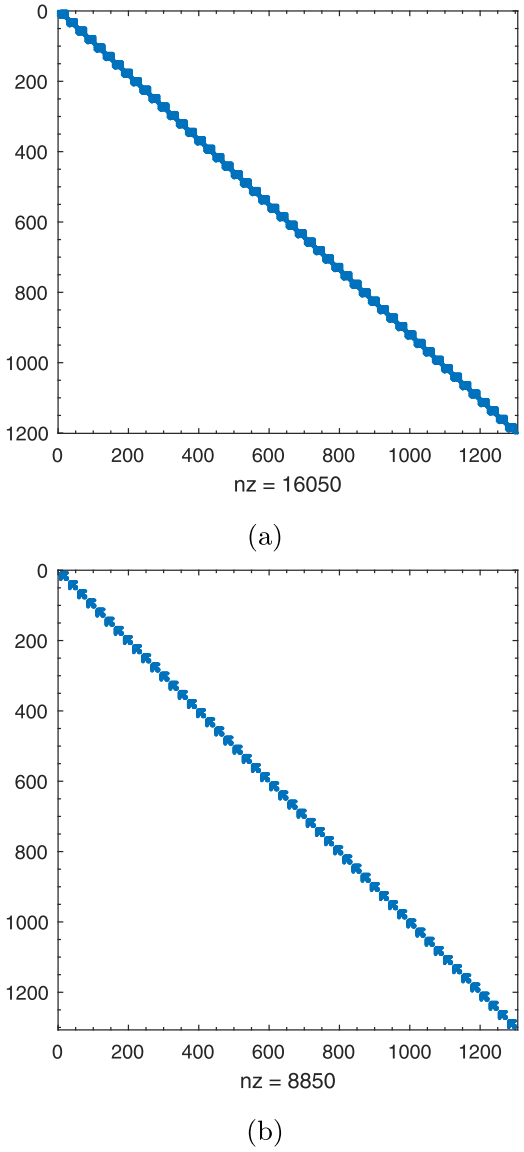

Fig. B1. Karush–Kuhn–Tucker (KKT) sparsity patterns for discretized NLP for the *Pf*BAL-catalyzed EPF formulation, where nz means the number of non-zeros. Jacobian matrix (a); Hessian matrix (b).

References

Andersson, J.A.E., Gillis, J., Horn, G., Rawlings, J.B., Diehl, M., 2018. CasADi – a software framework for nonlinear optimization and optimal control. Math. Program. Comput. doi:10.1007/s12532-018-0139-4.

Aydin, E., Bonvin, D., Sundmacher, K., 2018. NMPC using Pontryagin's Minimum Principle-Application to a two-phase semi-batch hydroformylation reactor under uncertainty. Comput. Chem. Eng. 108, 47–56. doi:10.1016/j.compchemeng.2017.08.010.

Begemann, J., Ohs, R.B.H., Ogolong, A.B., Eberhard, W., Ansorge-Schumacher, M.B., Spiess, A.C., 2016. Model-based analysis of a reactor and control concept for oxidoreductions based on exhaust CO_2-measurement. Process Biochem. 51 (10), 1397–1405. doi:10.1016/j.procbio.2016.06.024.

Bergner, L., Kirches, C., 2018. The polynomial chaos approach for reachable set propagation with application to chance-constrained nonlinear optimal control under parametric uncertainties. Opt. Control Appl. Methods 39 (2), 471–488. doi:10.1002/oca.2329.

Bertsekas, D.P., Tsitsiklis, J.N., 2008. Introduction to Probability, 2nd Athena Scientific.

Biegler, L.T., 1984. Solution of dynamic optimization problems by successive quadratic programming and orthogonal collocation. Comput. Chem. Eng. 8 (3–4), 243–247. doi:10.1016/0098-1354(84)87012-X.

Biegler, L.T., 2007. An overview of simultaneous strategies for dynamic optimization. Chem. Eng. Process. 46 (11), 1043–1053. doi:10.1016/j.cep.2006.06.021.

Biegler, L.T., 2010. Nonlinear Programming. Society for Industrial and Applied Mathematics, Philadelphia doi:10.1137/1.9780898719383.

Boukouvala, F., Niotis, V., Ramachandran, R., Muzzio, F.J., Ierapetritou, M.G., 2012. An integrated approach for dynamic flowsheet modeling and sensitivity analysis of a continuous tablet manufacturing process. Comput. Chem. Eng. 42, 30–47. doi:10.1016/j.compchemeng.2012.02.015.

Boyd, S., Vandenberghe, L., 2018. Introduction to Applied Linear Algebra: Vectors, Matrices, and Least Squares. Cambridge University Press.

Ciriello, V., Di Federico, V., Riva, M., Cadini, F., De Sanctis, J., Zio, E., Guadagnini, A., 2013. Polynomial chaos expansion for global sensitivity analysis applied to a model of radionuclide migration in a randomly heterogeneous aquifer. Stochastic Environ. Res. Risk Assess. 27 (4), 945–954. doi:10.1007/s00477-012-0616-7.

Cuthrell, J.E., Biegler, L.T., 1987. On the optimization of differential-algebraic process systems. AIChE J. 33 (8), 1257–1270. doi:10.1002/aic.690330804.

Diehl, M., Bock, H.G., Kostina, E., 2006. An approximation technique for robust nonlinear optimization. Math. Program. 107 (1–2), 213–230. doi:10.1007/s10107-005-0685-1.

Dudding, T., Houk, K.N., 2004. Computational predictions of stereochemistry in asymmetric thiazolium- and triazolium-catalyzed benzoin condensations. Proc. Natl. Acad. Sci. 101 (16), 5770–5775. doi:10.1073/pnas.0307256101.

Duff, I.S., 2004. MA57—a code for the solution of sparse symmetric definite and indefinite systems. ACM Trans. Math. Softw. 30 (2), 118–144. doi:10.1145/992200.992202.

Emenike, V.N., Schenkendorf, R., Krewer, U., 2018. A systematic reactor design approach for the synthesis of active pharmaceutical ingredients. Eur. J. Pharm. Biopharm. 126, 75–88. doi:10.1016/j.ejpb.2017.05.007.

Freund, H., Sundmacher, K., 2008. Towards a methodology for the systematic analysis and design of efficient chemical processes. Chem. Eng. Process. 47 (12), 2051–2060. doi:10.1016/j.cep.2008.07.011.

Galvanin, F., Barolo, M., Bezzo, F., Macchietto, S., 2009. A backoff strategy for model-based experiment design under parametric uncertainty. AIChE J. 56 (8), 2088–2102. doi:10.1002/aic.12138.

Hartman, R.L., 2012. Managing solids in microreactors for the upstream continuous processing of fine chemicals. Org. Process Res. Dev. 16 (5), 870–887. doi:10.1021/op200348t.

Hildebrand, F., Kühl, S., Pohl, M., Vasic-Racki, D., Müller, M., Wandrey, C., Lütz, S., 2007. The production of (R)-2-hydroxy-1-phenyl-propan-1-one derivatives by benzaldehyde lyase from Pseudomonas fluorescens in a continuously operated membrane reactor. Biotechnol. Bioeng. 96 (5), 835–843. doi:10.1002/bit.21189.

HSL (2007). A collection of Fortran codes for large scale scientific computation,. http://www.hsl.rl.ac.uk/.

Julier, S.J., Uhlmann, J.K., 1996. A general method for approximating nonlinear transformations of probability distributions. Robotics Research Group, Department of Engineering Science, University of Oxford, Oxford, OC1 3PJ United Kingdom.

Kim, K.-K. K., Braatz, R.D., 2013. Generalised polynomial chaos expansion approaches to approximate stochastic model predictive control. Int. J. Control 86 (8), 1324–1337. doi:10.1080/00207179.2013.801082.

Kiparissides, A., Kucherenko, S.S., Mantalaris, A., Pistikopoulos, E.N., 2009. Global sensitivity analysis challenges in biological systems modeling. Ind. Eng. Chem. Res. 48 (15), 7168–7180. doi:10.1021/ie900139x.

Kokova, M., Zavrel, M., Tittmann, K., Spiess, A.C., Pohl, M., 2009. Investigation of the carboligase activity of thiamine diphosphate-dependent enzymes using kinetic modeling and NMR spectroscopy. J. Mol. Catal. B 61 (1–2), 73–79. doi:10.1016/j.molcatb.2009.02.021.

Koller, R.W., Ricardez-Sandoval, L.A., Biegler, L.T., 2018. Stochastic back-off algorithm for simultaneous design, control, and scheduling of multiproduct systems under uncertainty. AIChE J. 00. doi:10.1002/aic.16092.

Lerner, U.N., 2002. Hybrid Bayesian networks for reasoning about complex systems. Stanford University, Stanford, CA Ph.D. thesis..

Lin, N., Xie, X., Schenkendorf, R., Krewer, U., 2018. Efficient global sensitivity analysis of 3D multiphysics model for Li-ion batteries. J. Electrochem. Soc. 165 (7), A1169–A1183. doi:10.1149/2.1301805jes.

Marelli, S., Sudret, B., 2014. UQLab: a framework for uncertainty quantification in Matlab. In: Vulnerability, uncertainty, and risk: Quantification, mitigation, and management, pp. 2554–2563. doi:10.1061/9780784413609.257.

Mesbah, A., Streif, S., Findeisen, R., Braatz, R.D., 2014. Stochastic nonlinear model predictive control with probabilistic constraints. In: 2014 American Control Conference, pp. 2413–2419. doi:10.1109/ACC.2014.6858851.

Morales-Rodriguez, R., Meyer, A.S., Gernaey, K.V., Sin, G., 2012. A framework for model-based optimization of bioprocesses under uncertainty: lignocellulosic ethanol production case. Comput. Chem. Eng. 42, 115–129. doi:10.1016/j.compchemeng.2011.12.004.

Müller, M., Sprenger, G.A., Pohl, M., 2013. C–C bond formation using ThDP-dependent lyases. Curr. Opin. Chem. Biol. 17 (2), 261–270. doi:10.1016/j.cbpa.2013.02.017.

Ohs, R., Leipnitz, M., Schöpping, M., Spiess, A.C., 2018. Simultaneous identification of reaction and inactivation kinetics of an enzyme-catalyzed carboligation. Biotechnol. Prog. 1–34. doi:10.1002/btpr.2656.

Ohs, R., Wendlandt, J., Spiess, A.C., 2017. How graphical analysis helps interpreting optimal experimental designs for nonlinear enzyme kinetic models. AIChE J. 63 (11), 4870–4880. doi:10.1002/aic.15814.

Paulson, J.A., Mesbah, A., 2017. An efficient method for stochastic optimal control with joint chance constraints for nonlinear systems. Int. J. Robust Nonlinear Control 1–21. doi:10.1002/rnc.3999.

Peschel, A., Freund, H., Sundmacher, K., 2010. Methodology for the design of optimal chemical reactors based on the concept of elementary process functions. Ind. Eng. Chem. Res. 49 (21), 10535–10548. doi:10.1021/ie100476q.

Ploch, T., 2014. Model-based optimization of an enzyme-catalyzed reaction network. Rheinisch-Westfälische Technische Hochschule Aachen, Aachen, Germany Master's thesis..

Pollard, D.J., Woodley, J.M., 2007. Biocatalysis for pharmaceutical intermediates: the future is now. Trends Biotechnol. 25 (2), 66–73. doi:10.1016/j.tibtech.2006.12.005.

Price, J., Hofmann, B., Silva, V.T.L., Nordblad, M., Woodley, J.M., Huusom, J.K., 2014. Mechanistic modeling of biodiesel production using a liquid lipase formulation. Biotechnol. Prog. 30 (6), 1277–1290. doi:10.1002/btpr.1985.

Puschke, J., Zubov, A., Kosek, J., Mitsos, A., 2017. Multi-model approach based on parametric sensitivities – a heuristic approximation for dynamic optimization of semi-batch processes with parametric uncertainties. Comput. Chem. Eng. 98, 161–179. doi:10.1016/j.compchemeng.2016.12.004.

Rehrl, J., Gruber, A., Khinast, J.G., Horn, M., 2017. Sensitivity analysis of a pharmaceutical tablet production process from the control engineering perspective. Int. J. Pharm. 517 (1–2), 373–382. doi:10.1016/j.ijpharm.2016.11.064.

Saltelli, A., Chan, K., Scott, E.M., 2000. Sensitivity Analysis, 1st Wiley, New York.

Schenkendorf, R., 2014. A general framework for uncertainty propagation based on point estimate methods. In: Second European Conference of the Prognostics and Health Management Society, PHME14.

Schenkendorf, R., Xie, X., Rehbein, M., Scholl, S., Krewer, U., 2018. The impact of global sensitivities and design measures in model-based optimal experimental design. Processes 6 (4), 27. doi:10.3390/pr6040027.

Shi, J., Biegler, L.T., Hamdan, I., Wassick, J., 2016. Optimization of grade transitions in polyethylene solution polymerization process under uncertainty. Comput. Chem. Eng. 95, 260–279. doi:10.1016/j.compchemeng.2016.08.002.

Sin, G., Gernaey, K.V., Lantz, A.E., 2009. Good modelling practice (GMoP) for PAT applications: propagation of input uncertainty and sensitivity analysis. Biotechnol. Prog. 25, 1043–1053. doi:10.1021/bp.166.

Sobol, I.M., 1993. Sensitivity estimates for nonlinear mathematical models. Math. Modell. Comput.Exp. 1 (4), 407–414.

Srinivasan, B., Bonvin, D., Visser, E., Palanki, S., 2003. Dynamic optimization of batch processes: II. Role of measurements in handling uncertainty. Comput. Chem. Eng. 27 (1), 27–44. doi:10.1016/S0098-1354(02)00117-5.

Stillger, T., Pohl, M., Wandrey, C., Liese, A., 2006. Reaction engineering of benzaldehyde lyase from *Pseudomonas fluorescens* catalyzing enantioselective C-C bond formation. Org. Proc. Res. Dev. 10 (15), 1172–1177. doi:10.1021/op0601316.

Streif, S., Kim, K.K.K., Rumschinski, P., Kishida, M., Shen, D.E., Findeisen, R., Braatz, R.D., 2016. Robustness analysis, prediction, and estimation for uncertain biochemical networks: an overview. J. Process Control 42, 14–34. doi:10.1016/j.jprocont.2016.03.004.

Telen, D., Vallerio, M., Cabianca, L., Houska, B., Van Impe, J., Logist, F., 2015. Approximate robust optimization of nonlinear systems under parametric uncertainty and process noise. J. Process Control 33, 140–154. doi:10.1016/j.jprocont.2015.06.011.

Visser, E., Srinivasan, B., Palanki, S., Bonvin, D., 2000. A feedback-based implementation scheme for batch process optimization. J. Process Control 10, 399–410. doi:10.1016/S0959-1524(00)00015-9.

Wächter, A., Biegler, L.T., 2006. On the implementation of an interior-point filter line-search algorithm for large-scale nonlinear programming. Math. Program. 106 (1), 25–57. doi:10.1007/s10107-004-0559-y.

Wang, Z., Ierapetritou, M., 2018. Global sensitivity, feasibility, and flexibility analysis of continuous pharmaceutical manufacturing processes. In: Singh, R., Yuan, Z. (Eds.), Process Systems Engineering for Pharmaceutical Manufacturing. In: Computer Aided Chemical Engineering, vol. 41. Elsevier, pp. 189–213. doi:10.1016/B978-0-444-63963-9.00008-7.

Woodley, J.M., 2008. New opportunities for biocatalysis: making pharmaceutical processes greener. Trends Biotechnol. 26 (6), 321–327. doi:10.1016/j.tibtech.2008.03.004.

Xie, X., Krewer, U., Schenkendorf, R., 2018a. Robust optimization of dynamical systems with correlated random variables using the point estimate method. IFAC-PapersOnLine 51 (2), 427–432. doi:10.1016/j.ifacol.2018.03.073.

Xie, X., Ohs, R., Spieß, A., Krewer, U., Schenkendorf, R., 2018b. Moment-independent sensitivity analysis of enzyme-catalyzed reactions with correlated model parameters. IFAC-PapersOnLine 51 (2), 753–758. doi:10.1016/j.ifacol.2018.04.004.

Zavrel, M., Schmidt, T., Michalik, C., Ansorge-Schumacher, M., Marquardt, W., Büchs, J., Spiess, A.C., 2008. Mechanistic kinetic model for symmetric carboligations using benzaldehyde lyase. Biotechnol. Bioeng. 101 (1), 27–38. doi:10.1002/bit.21867.